MARINE ICING SENSOR DESIGN USING CAPACITIVE TECHNIQUES

A thesis presented to the School of Graduate Studies of

Memorial University of Newfoundland in partial fulfillment of the requirement leading to the

award of a Masters in

ELECTRICAL ENGINEERING

By

Department of Electrical and Computer engineering

Faculty of Engineering & Applied Science

Memorial University of Newfoundland

May 30th 2017

ABSTRACT

The Marine Icing project, in industrial collaboration with Statoil, explores and develops in-depth research on marine icing phenomena, and the appropriate sensor technology to detect ice accretion in marine and offshore environments. The overall project includes detailed analytical concepts, simulations, and experiments of on and off deck ice accretion activities in the form of wave breakup and droplet freeing phenomena.

Part of the project is dedicated to developing appropriate low cost sensors for ice accretion detection in these harsh environments. Proposed sensors should be autonomous and easy to modify. After examining the available ice detecting systems, it was decided to explore capacitive techniques, a concept that have been used in other industrial applications like tilt sensing, liquid level sensing, and accelerometers. However, the capacitive sensing technique has not been explored for marine ice detection and therefore will be developed in this thesis.

A capacitive based sensor is simulated, designed, tested, and documented in this thesis. The proposed sensor consists of a copper tracing on a PCB, capacitance to digital converter circuit and a microcontroller. The whole system runs on a simple battery system or powered by a programming cable, depending on the area of deployment. The microcontroller controls the capacitance to digital converter circuit as well as the temperature sensing circuit. Additionally, this research compares the change in capacitance observed with the change in ice thickness; proper sensor calibration is drawn from this result. The system is used to test ice accretion due to fresh and saline water, observation and conclusions are made based on the data obtained. This thesis focuses on developing a technical start up point for capacitive marine ice sensing.

Dedication

This thesis is dedicated to my beloved family

ACKNOWLEDGEMENTS

In the present world of competition, there is a race of existence in which those who have will to come forward succeed. Project like this is an academic background to much larger industrial application, and a bridge between theoretical and practical applications. Masters in Engineering is a tedious, challenging, but enjoyable part of my education; hence, several people have played a vital role in making this happen. Every effort and support although the years are well appreciated. This research has been supported by Statoil, RDC and MITACS.

First of all I would like to thank the supreme power the God Almighty for guiding me to walk on the right path of life, encouraging me when I needed divine support and keeping me healthy though my 7 years in Engineering. Without his grace, this project will not be a reality.

I would like to thank my supervisor, Dr. Vlastimil Masek for keeping me in the right track when faced with unexpected challenges, providing me with advice and also helping me through this research especially when I am running of ideas. Dr. Masek has been my instructor through my undergraduate electrical engineering program and I am fortunate to have him as my supervisor though my graduate program. I am forever grateful for his kind and patient attitude in providing me alternate solutions during my vulnerable and frustrating times as a student.

I would also like to thank my co-supervisor, Dr. Yuri Muzychka, for his advice, and support during the course of this program, his dedication to the marine icing team has been a breath of fresh air, and I personally have gained immensely leadership skills and some knowledge in the mechanical engineering field relating to marine icing. His positive attitude throughout the

Table of Figures

Table of Tables

List of Abbreviations

AC   Alternating Current

DC   Direct Current

ADC   Analogue to Digital Converter

CMOS   Complementary Metal Oxide Semiconductor

DC   Direct Current

IC   Integrated Circuit

IEEE   Institute of Electrical and Electronics Engineers

IT   Information Technology

MEMS   Micro-Electro-Mechanical Systems

MOS   Metal Oxide Semiconductor

MOSFET   Metal Oxide Semiconductor Field Effect Transistor

NMOS   n-channel MOSFET

PCB   Printed Circuit Board

PMOS   p-channel MOSFET

PSU   Practical Salinity Unit

I   Current

V   Voltage

C   Capacitance

R   Resistance

Marine Icing Sensor Design Using Capacitive Techniques

Table of Contents

Chapter 1

Introduction

Marine atmospheric conditions in arctic regions pose a number of problems that are unique to the cold regions around the world. The most intriguing problem is presented by sub-freezing air temperatures combined with wave actions and their impact with the offshore structures. In Canada, ice loads pose the most imminent danger, especially in offshore oil drilling operations. Most of alternative Canadian Oil and Gas wells are offshore, and at least 200 wells have been successfully drilled with high rate of success in offshore Newfoundland till date [1]. Offshore vessels and structures are used during production and transportation phases of these wells. Furthermore, various types of vessels are used to transport oil and offshore workers to and from these sites. FPSOs (Floating production storage and offloading) are also used in these areas, and other moving vessels such as ice breakers and transport vehicles are often employed during these activities. Danger due to super structure ice accretion or freezing spray has been the main concern for arctic vessels due to ice loads.

In Canadian arctic waters, vessels operating in late fall and winter are likely to experience some degree of icing phenomenon in exposed areas of the structures such as decks, railing and bulwarks. Marine icing could seriously blight vessel operation, safety, and stability [2]. Ice loads could alter the dynamics of ship movement as the center of gravity is raised, which could lower

the speed of the ship and cause problems when manoeuvring. Furthermore, ice loads increase the overall weight of the ship and increase the cost of operation.

Unfortunately, this natural phenomenon is not preventable with the existing technology; the only remedies is to provide suitable means to provide accurate information on allowable ice loads on a vessel and provide means to remove them. In depth ice accretion research is underway in recent years; many government funded institutions in the country embark on research in this area. However, ways to mitigate the effect of marine icing are conducted with limited success so far. Most operational vessels resolve in a routine check of the structure surfaces and mechanical removal of ice.

Ice accretion is a slow and continuous process which necessitates proper investigation because of the hazards it might cause. In Canadian arctic waters, most icing on vessels can result from saltwater moisture and impinging freezing rain or wet snow known as spray icing. Ice accretions in ships are as a result of fast sea spray from sea wind and wave generated sprays in form of super cooled droplets [3] . Spray icing can occur over time, under favourable cold temperatures as these super cooled droplets freezes onto parts of the vessel before the runoff time elapses [2]. Reports show that different areas of the arctic region experience various lengths of natural icing yearly, with most areas experiencing less than 25 hours and some experiencing more icing periods. Baffin Bay, Davis Strait, and Amundsen Gulf near Cape Parry experience 25 to 50 hours of icing annually. Further north, areas like Brevoort and resolution Islands icing may occur for as many as 100 hours each year [2]. The marine icing also includes the ocean spray introduction with the frozen structure and thus this phenomenon can occur at much southern latitude.

The emerging field of ice detection and removal is slowly gaining interest and most offshore vessels operations are seeking proper means to detect icing on a surface in real time. Information gained is used to design techniques or to apply proper measures to remove marine ice on structures. In order to design systems for ice accretion detection, an understanding of the dielectric properties of ice and water is vital. The purpose of this thesis is to provide a workable sensor module for ice accretion detection using capacitive techniques. This thesis demonstrates the overall engineering design procedures of the sensor module. In addition, the parts selection criteria will also be discussed and a final prototype of the system will be presented at the end of the thesis. Experimental results and discussion of the overall contribution of the research is documented in this thesis.

1.0 Thesis outline

Chapter 2 of this thesis provides the necessary background information and literature review of the overall concept. This chapter covers an in-depth research on state of the art direct ice accretion detection methods, comparisons between them, and some of the limitations are discussed. The basic physics and technical background of capacitances and dielectrics will be presented in the Chapter 3. Additionally, Chapter 3 presents the relationship between these electrical parameters and electric field during ice sensing. Furthermore, Chapter 4 documents all the capacitive plate electrostatics simulation using COMSOL Multiphysics and useful results needed to validate the actual experiments. Chapter 5 of this thesis presents the main sensor electronics, design, and schematics, this chapter also contain the full design and component selection criteria documentation. Chapter 6 discusses the final system prototype on a proto-

board. This prototype is the final design stage needed in this thesis, further work on this prototype is included in the last chapter.

The prototype designed in this thesis is used as it is for atmospheric and sea icing accretion experiments. Discussions of these results are presented in Chapter 7 of this thesis; the summary of the operating limits and the effectiveness of capacitive sensing for marine icing are also presented in this chapter. Chapter 8 presents an important component of the thesis where a more realistic analysis using Statistical methods to analyse a multiphase phase medium. Chapter 9 summarises the research conclusion, contribution and future work.

Additionally, this thesis contains an appendix section of the full microcontroller codes, header files, and data acquisition codes used in obtaining the results discussed in this thesis.

Chapter 2

Literature Review

2.0 Introduction

Ice accretion is a very complex phenomenon; hence an in-depth understanding provides a way forward in designing proper systems for marine ice sensing. This section reviews the conducted researches on the basic impact of icing, icing accretion process, and the state of the art ice detection sensors and their various applications. Most offshore operations and transportation activities take icing phenomenon seriously and often work out ways to remove, or mitigate icing on and off deck of marine vessels. This section discusses the impact of marine icing and presents various ice sensors commercially available and their method of operation. In addition, some of these sensors have been designed but never tested in marine environments, and some have been tested but have not provided meaningful results of offshore ice thickness. On shore, most of these sensors have shown some promise in ice accretion detection. The general impact of icing will be presented beforehand to provide a better undemanding of the research problem statement.

2.1 General Impact of Icing

Icing on surfaces of ships and offshore structures in sub-arctic regions impose a dead load that could affect the economics of operating the structures during the winter months. Ice loads have also been proved to be dangerous to the safety of the personnel as smaller transport vessels could

capsize when ice loads are unevenly distributed on the vessel. Ice loads could accumulate on stairs, handrails, decks, and other exposed areas of the offshore structure; without proper measures in place to control or remove them, and ice loads could grow a hundreds of centimeters thick posing some adverse problems. The rate of icing in marine structures increases with an increase in sea spray, which in return depends on other environmental conditions such as temperature, relative humidity, wind speed and wind direction etc.

Icing in offshore structures can lead to increased cost of operation in terms of fuel cost, maintenance and some engineering considerations for arctic chipping operations. Due to high ice accretion rate transportation routing might be considered which might not be cost effective all the time. To maximise the performance of these offshore vessels and structures, meteorological instruments are generally mounted on meteorological towers to measure environmental parameters such as humidity, ambient air temperature, wind speed, and direction. These instruments can only provide information on the environmental conditions leading to ice accretion but do not provide a good analysis on the amount of ice presently on the structure. In arctic regions, ice loads problems are caused mainly from atmospheric icing [4]. Atmospheric icing is the process by which ice deposits and grows on a surface or structure as a result of exposure to atmospheric conditions. There are two types of atmospheric icing, in-cloud icing and precipitation icing. In-cloud icing occurs when super cooled water drops impact on the surface of a structure resulting in the formation of ice; these droplets could results from wave breakups, and in cloud icing typically forms on-deck on marine vessels. Precipitation icing is formed due to wet snow or freezing rain, this is occurs very often in aircraft wings in higher altitudes [4].

2.2 Methods of Ice detection

Methods of ice detection are application dependent and also depend on the variables needed to be detected. Some ice sensors simply measure the environmental conditions leading to ice accretion such as temperature, wind speed, precipitation, and relative humidity. These are important parameters used to determine icing conditions. On the other hand, some sensors measure the ice thickness as the icing occurs. Methods of ice accretion detection are broadly divided into direct and indirect methods of ice detection.

2.2.1 Indirect method of ice detection

The indirect method of ice detection involves measuring the atmospheric conditions that leads to prediction of an upcoming event. Climate conditions such as relative humidity, atmospheric temperatures, and wind velocity are some conditions that could lead to icing event in open waters. Data collected from various test sites are used alongside some Pre-determined Empirical models to forecast upcoming events. Fikke *et al* reported some useful results by using inventories of past and present atmospheric conditions from various test sites; these results are used in predicting icing phenomena in various European cities [4]. Some researchers have built their predictive models based on indirect method of ice detection, but as a result of global warming, these results have often proven to be inaccurate and needed to be updated more frequently, for this reason, more useful results and conclusions are sought after.

2.2.2 Direct method of ice detection

The direct method of ice involves a systematic ice measurement in real time as ice accretion activity occurs. This is based on detecting change in physical and chemical properties during ice build-up. Parameters such as mass, dielectric constants, conductivities or even inductance

properties of ice are often detected using some known sensors. Research also shows that these parameters varies from one type of ice to another, hence it provides a way to distinguish various forms of ice. Li *et al* proposed a system applies fibre optic technology to measure the intensity of the absorbed or scattered energy when a beam passes through an ice sheet [5]. The result of the research is able to distinguish between glazes, rime ice and snow. This thesis provides a close look at the existing commercially available ice sensors. Although, this thesis explores primarily the direct methods of ice accretion, commercially available sensors are for both direct and indirect ice accretion sensors are reviewed.

2.3 Some Icing Sensors

There are currently no proven sensors for offshore marine applications capable of detecting ice accretion without the need for constant routine maintenance. Some advancement has been made in producing sensors for ice detection, however over the years most icing sensors have been tailored towards the aerospace industries. Very light ice accretion occurs in aircraft wings as a result of very high velocity and altitude which they travel. By design, these sensors are not adaptable for marine icing where heavy ice accretion occurs. Marine icing conditions also present the harshest environment possible; therefore, the sensor robustness is paramount. This thesis will cover a brief review of the available sensors.

2.3.1 Goodrich ice detector model 0871LH1

The Goodrich ice detector model 0871LH1 sensor is applicable in the aviation industry. It is a low power sensor manufactured by UTC aerospace systems and this sensor is currently under improvement. The Goodrich ice detector model 0871LH1 detects icing accretion on the probes

by monitoring the change in frequency as the mass of ice on the surface increase with time [6]. The shift in resonance frequency of the probe is monitored as it reaches or approaches its set point; this triggers the de-icing mode for a certain time to remove the icing on the probes. One of the short comings of this sensor is its inability to distinguish between water, air, and ice. Several experiments also conducted by the manufacturer's shows that the Goodrich ice detector can only measure very thin ice accurately. This ice sensor also has not been tested in offshore marine environments, but it has shown some proven applicability in turbine blades, transmission lines and antennas [6]. Additionally, newer model sensors like the Combitech ice monitor can monitor heavier ice thickness and has been tested in the power industry.

2.3.2 Combitech Ice Monitor

The Combitech Ice monitor is manufactured by Combitech, and industrially marketed and applied by SAAB technologies, built based on the ISO 12494 standard. This sensor is originally designed and tested for icing surveillance on power lines as most high voltage power line in cold regions experience sever ice thickness in the winter. The operation of the Ice monitor is one of the simplest in the icing sensor technology where the mass of ice accumulated on a surface is measured gravitationally. The sensor has very low power performance by design which employs a freely rotating steel pipe resting on a rod placed on load cells. In principle, the load cells record the ice loads as icing activates occurs on the freely rotating steel pipes [7]. Furthermore, the sensor has a moving mechanical part which limits its application in very harsh marine environments. Additionally, unlike the ice detector model, the Combitech has no means of de-icing like the ice detector model 0871LH1.

2.3.3 Instrumar Ice Sensor

The Instrumar limited ice sensor is the only sensor that combines the direct and indirect method of ice accretion. The principle of operation involves measuring the surface temperature and electrical impedance [8]. Substance that enters or contacting the sensor enters the electromagnetic field, and the change in electromagnetic field is detected. The device is programmed with a pre-set set point for icing condition and a notification is obtained when this set point is reached. Also, when an expected icing condition is reached, the Instrumar ice sensor triggers an alarm in form of an electrical signal. This same signal is used to trigger the heating devices and notification systems. The device also interfaces with full software for real time data acquisition [9]. The Instrumar measures moisture content, temperature, conductivity and is highly adapted in aerospace applications.

2.3.4 HoloOptics T40-series icing rate sensors

HoloOptics manufactures the T40-series which is an improved modification from the old T20 series. This sensor design is unique and comprises a four curved bars made of stainless steel with infrared probes installed. Each curved bar has a photo detector and a probe built as a single unit. The probe emits infrared light that is reflected by a reflector and the ice thickness is determined by the amount of light that bounces back to the probe. The HoloOptics T20 is an older series that has been tested in various sites to measure ice levels of about 0.01mm thick, reasonable results were obtained. The sensor is designed to produce an indication in form of a programmed alarmed if 95% of the probe is covered with 50μm to 90μm of any type of ice [4]. The de-icing mechanism in the sensor is deactivated in temperatures above $+10^o$C so that heating is only

required when needed. De-icing time while the probe heating is activated depends on some environmental factors such as surface temperature, air temperature, ice thickness, and the insulted melting power [10]. This measurement is a hundred times of the order of magnitude less than the application presented in this thesis; hence, this is not suitable for marine icing.

2.4 Capacitive Ice Sensor

Capacitive ice sensors are designed to generate an electric field cloud which is used to detect the presence of dielectric materials that enter the region of the field. This change in capacitance is used to determine the material in the region. *Tiuri et.* al. [11] conducted experiments in this area, results shows that the dielectric constant of dry snow is determined by its density and that for wet snow, is determined by the imaginary part of the density measurement. The experiment further proved that there is some volumetric wetness dependence in increasing the real part of the density measurement, due to liquid water. In other words, the presence of liquid water will increase the dielectric property of dry snow. Furthermore, the electrical properties of ice have also been further investigated and have been used to measure the presence and thickness of ice on a surface, as presented by Evanes [12]. Weinstein [13], Kwadwo [14] and Jarvinen [15].

2.4.1 Cylindrical probes ice detection technique

The experiment conducted by kwadwo [14], using two aluminum based cylindrical probes to form a capacitive sensor probe. The experimental report shows that the fringing electric field between two electrical charged cylindrical probes can be disrupted by the presence of ice; this increases the capacitance of the probe pair and decreases the resistance. This experiment is conducted in a controlled environment where super cooled droplets are directed towards the

probes perpendicular to the electric field lines. The super cooled droplets are allowed to grow on the probes in controlled conditions as shown in Figure 2.1 and 2.2 below, The ratio of the increase in capacitance measures at a particular thickness of ice compared to clean air is used as a measure to determine the thickness of ice on the probes. The resistance between the two probes increases with an increase in ice accretion as a result of a decrease in the air gap. The change in capacitance, resistance, and voltage between the two probes were also investigated for various types of ice. Rime, frazil, and glaze ice were also compared and the resulting capacitances were analysed. This experiment proves to be consistent with the expected result of capacitive sensing. Results also showed that an increase in the salt content of the ice results in a decreased DC voltage, but does not particularly change the dielectric property of the ice which effects a change in capacitance. This is an important conclusion when applying capacitive sensor in marine offshore applications. This particular sensor was designed and tested in a lab scale; hence it also measures ice thickness for a few millimetres. The EAG 200 possesses the ability to measure heavier ice thickness.
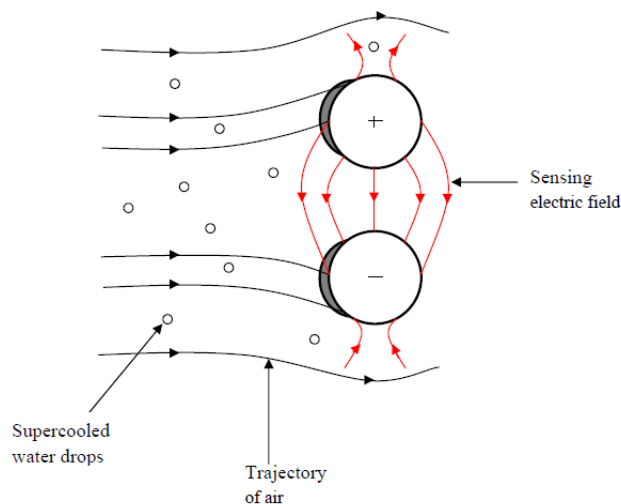
Figure 2.1 Super cooled droplets approaching a capacitive probe

Figure 2.2 Ice accretion on parallel cylindrical probes.

2.4.2 EAG 200

The EAG 200 is a German engineered icing sensor. The ice load sensor EAG 200 is an automatic icing measurement device that has been used in various European measuring sites to determine ice loads based on the weight of ice accumulated on a vertical pole using an electromechanical scale system [16]. The EAG 200 measures within a range of 0 to 10kg with an accuracy level of ± 50 g. The ice poles are has a diameter of 0.035m and a pole length of 1m made of PVC. Additionally, the comparison of EAG 200 results with those of manually operated poles show the reliability of EAG200's data. Data collected over a long period of time shows that the EAG works well for small amount and operate well for short icing periods [4]. All weight measurement based ice sensor work well in state environments such as weather stations and test sites. However, a floating marine structure presents a dynamic condition as a result of strong wind gusts and structural vibration, which rules out load sensors in our application.

Chapter 3

Technical background: Capacitive Sensing

3.0 Introduction

Capacitive sensing technology has grown in popularity in recent years to replace generic optical detections and mechanical sensing techniques in various engineering applications. Capacitive sensing technique is applied in direct sensing applications such as chemical composition, electric field and liquid level sensing. Industrial applications of these sensing techniques include motion detection, acceleration, moisture, water and ice detection. In advanced applications, this technique has also been used to detect gas composition and also provides alerts on the presence of hazardous gases in an environment.

The design of capacitive sensors often have two sensing electrodes in a single dielectric, where one electrode is grounded relative to the other excited electrode, which turns the capacitance changes into voltage variations. The next section introduces capacitances and dielectrics and also shows the basic physics behind capacitances, this also illustrates the concept of dielectrics.

3.1 Capacitance and Dielectrics

In electronics engineering, the electrical concept of capacitances is based on capacitors. As simple as this application might seem, it is a used as building block in many electronics design. Capacitors are electrical passive elements which have the ability to store electric charge; this

electric charge creates a potential difference across the positive and negative plates that comprise a capacitor. The simplest form of capacitor consists of two non-contact parallel plates of known metal materials electrically separated by air. Electrolytic capacitors could be separated by other insulating materials such as ceramic or wax; such materials are known as dielectrics. Capacitators vary in shape and size depending on the application and the voltage rating which they are designed for; generally, but the basic internal configuration is unchanged. Figure 3.1 [14] shows the basic setup of a capacitor, it comprises of two conductors carrying equal but opposite charges, and the electric field interaction often starts from positive plate and terminates in the negative plate.
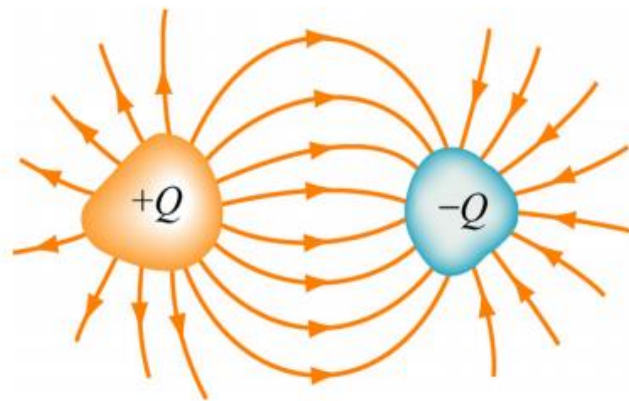
Figure 3.1 Basic configuration of a capacitor

There are two states of a capacitor, the charge state and the uncharged state. In the uncharged state, the charge on either one of the conductors is zero; this means that there are no electrons moving from the positive plate to the negative plate at this time. A charging process occurs when a direct current is placed across the capacitive plates. During the charging process, a charge Q is moved from one conductor to the other one, the charged conductor assumes a positive charge +Q, and the other a negative charge -Q . During this process, a potential difference is created

across the plates and the positively charged plate is said to be at a "higher potential" and the negative charged plate at a "lower potential". The flow of DC current through the capacitor is impeded by the insulating layer; the process of charge exchange presents a voltage across the plates in form of an electrical charge, here the capacitor is said to "store" the charge [17].

The presence of a steady DC current means the capacitive plates remain charged, until the capacitor reaches its steady state condition, and the charge also increases with the voltage. There are also various electrical methods to discharge a capacitor which will be discussed in later sections.

3.2 Electric Field

The Electric field effect is always associated with the capacitance of a capacitor depending on the type of dielectrics in between the plates. The voltage applied to the end of the sensing plates produces an electric field from the surfaces. These field lines define the capacitance between a pair of conductors in a much complex manner. Ideally, the electric field should be contained within the space between the sensing plates and the target material. In the case of an ideal capacitor, the dielectric will be assumed to be a vacuum, which allows the materials to be detected based on their dielectric properties as they "break" the electric field lines. Although there exist some other capacitor topology such as the cylindrical capacitors and line capacitors, but the scope of this thesis is concerned with two parallel conductors which are close together with the lines of electric field arising from one conductor which terminates on the neighbouring conductor in a small distance of separation. Figure 3.2 [18] shows a simple two parallel plate capacitor in vacuum with area A and distance of separation d, the capacitance could be computed by assuming one plate carry a charge +Q and the other plate –Q; and all field lines originate at

the positive plate and terminates at the negatively charged plate. The relationship between the electric field and the surface density is given by:

$$E = \frac{\sigma}{\varepsilon_0}$$

(3-1)

Charge density also related to the charge Q and the area A by

$$\sigma = \frac{Q}{A}$$

(3-2)

In this case, the direction of the electric field is ignored for a uniform electric field, assuming it is very nearly true for plates whose dimensions are large compared to their separation [18].
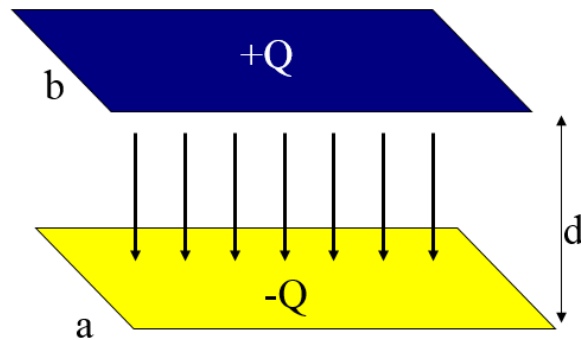
Figure 3.2 Configuration of a parallel plate capacitor

Often, the voltage difference V_{ba} between the two plates is expressed in terms of work done on a single charge as it moves from the positive plate to the negative plate. The work done by this charge is given by

$$V_{ab} = \frac{work\ done}{charge} = \frac{Fd}{q} = Ed$$

(3-3)

The perimeter for measuring the capacity of a conductor to store charge is called the *capacitance* and denoted by *C*. By definition, the capacitance of a charge is the ratio of the charge stored to the potential difference between the two plates as generated by the charge.

$$C = \frac{Q}{V_{ab}}$$

A good storage device should have high capacitance and high work done per charge; hence, from equation (3-2) and (3-3) capacitance can be expressed as:

$$C = \frac{Q}{Ed} \qquad (3\text{-}5)$$

Combining (3-1) and (3-5), a more compact equation for capacitance as

$$C = \frac{Q\varepsilon o}{\sigma d} = \frac{QA\varepsilon o}{Qd} = \frac{A\varepsilon o}{d} \qquad (3\text{-}6)$$

Additionally, in view of the equation above, an increase in capacitance is caused by an increase in charge stored in the capacitor which in turn results in an increase in the potential difference between the plates. From equation (3-5), this will in effect result in an in increase in the electric field.

This thesis will explore mainly the concept related to the effect of dielectrics on capacitance. As explained, a dielectric is a non-conducting material placed between a capacitive plate, and this often increases the capacitance.

$$E_{dielectric} = \frac{E_0}{k} \qquad\qquad\qquad (3\text{-}7)$$

$$V_{dielectric} = \frac{V_0}{k} \qquad\qquad\qquad (3\text{-}8)$$

The equation shows that the potential difference across free space is higher than the potential difference with a real dielectric. From (3-4)

$$C = \frac{Q}{V_{ab}} = k\frac{Q}{V_o} = kC_o \qquad\qquad\qquad (3\text{-}9)$$

Hence, this will result into a higher capacitance.

Generally, this thesis fundamentally covers this principle as relevant to marine icing, the change in capacitance is expected to be higher as the electric field lines are broken in the presence of icing and these phenomena will be used to measure ice thickness. Simulation and experimental results will also be used to support these equations.

Chapter 4

Capacitive Sensor Trace Simulation Experiments

4.0 Introduction

This chapter begins with a discussion of the selection criteria for the copper plate materials. The selection process will explore various capacitive plate configurations and simulations in COMSOL Multiphysics.

4.1 Advantage of capacitive sensing

In designing sensors for harsh environments, the critical criteria to consider are cost, robustness, and adaptability. Capacitive sensing is advantageous over all other types of sensing method due to the following reasons.

- Simplicity and very low cost to build.

- Capacitive sensing does not involve any moving, rotating, or vibrating mechanical parts which after some tear and ware could reduce efficiency and could also damage the system. Over time, this will increase the operation and maintenance cost of the whole ice detection system.

- Capacitive sensing involves very low power electronics in the overall design; this is due to the simplicity of the system.

- Marine icing sensor should be easily deployable in harsh environments with very little supervision. Sub-zero temperatures does not have an adverse effect on capacitive sensing. For this reason, it is much convenient to deploy on offshore rigs and vessels, and monitoring this sensors will require very little technical expertise.

- Due to the simplicity of the system, capacitive sensing has very low maintenance costs. Dust or debris could be easily cleaned off the surface when there is no ice accretion.

The above advantages outweigh its inability to measure very thick ice load like the ultrasonic sensing [20], as illustrated in the literature review of this thesis. Although there is no off the shelf capacitive sensor for marine icing available, and very little work or research has been done in this area to improve the ice sensing capability of capacitive sensors this technique of ice sensing still remains and ideal economical choice for low costs, ice sensing for offshore vessels. Unfortunately there is no literature comparison between the performances of other types of sensing techniques against the capacitive sensing technique as this technique has not been explored for offshore harsh weather applications.

4.2 Capacitive Sensor Topology

Generally speaking, the topology chosen for capacitive sensors are application dependent. A careful review of the material to be sensed would be done before choosing a topology. The sensor topology selected for marine applications depends on:

- Desired Sensitivity,

- Distance of Sensor-to-Target, and

- Dielectric constant of the target material.

The basic topology for capacitive sensing includes.

- Parallel Plates

- Parallel fingers

- Single sensors (used for human recognition).

4.2.1 Parallel Plates

The parallel plate topology works exactly as the parallel plate capacitor explained in the previous section. For parallel plate capacitance is, follows

$$C = \frac{\varepsilon\,A}{d} = \frac{k\varepsilon_0 A}{d}$$
(4-1)

Where

C is the overall capacitance (Farads)

A is the Area (m^2)

d is the distance of separation (m)

ε_0 is the permittivity of free space given by 8.854 x 10-^{12} F/m

ε_r is the relative permittivity of the dielectric material between the plates

Note: ε_r=1 for free space; ε_r>1 for all media, approximately= 1 for air.

This topology is used mainly in material sensing and analysis, and the change in capacitance between the plates will change accordingly depending on the difference between the dielectric constant for each material. Figure 4.1 [21], shows the typical arrangement of this topology. The material sensed is inserted between the sensing electrode and the ground electrode; this allows the material between to be identified by the dielectric property.

For this topology, a high resolution from the capacitance to digital converter interface circuit could be used to detect small changes in the dielectric. Hence, an increase in material thickness

results in an equal increase in capacitance and this observation is often proven by experiments. The capacitance could be related to the thickness of the material. This variable could be calculated by the difference between the dielectric properties of the material with air.
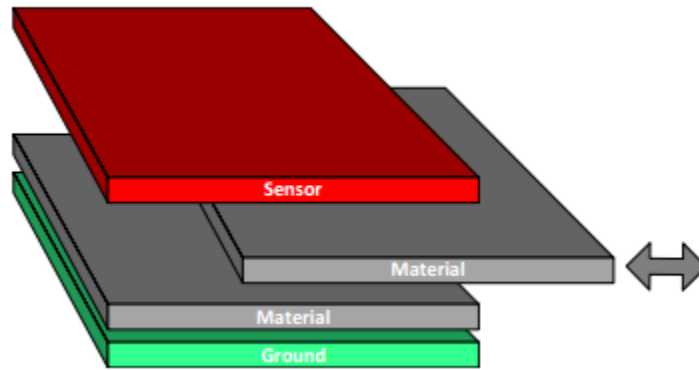
Figure 4.1 Parallel plate Topology for Material Analysis.

4.2.2 Parallel Fingers

As the name implies the parallel fingers topology is designed to be axial to the z-axis, the sensing materials and the fringing field lay in the same plane on the same side as shown in Figure 4.2 [22], this makes the fringing field dominance in this topology. In addition, unlike the parallel plate capacitance, the sensing materials lay in opposite sides creating smaller fringing field lines. The setup in the parallel fingers causes the electric field to be directed outwards towards the target which makes the parallel fingers a good candidate for liquid height measurement [13] [21]. The complexity of this typology makes calculating the capacitance very complicated as the area of the electric field fringing path is greater than the area between the ground and the charged surfaces. This thesis will explore an expert FEM software in COMSOL Multiphysics to perform a simulated will be used to provide a simulated capacitance for this topology, and the result will be trusted as a good measure with the actual laboratory measurement.
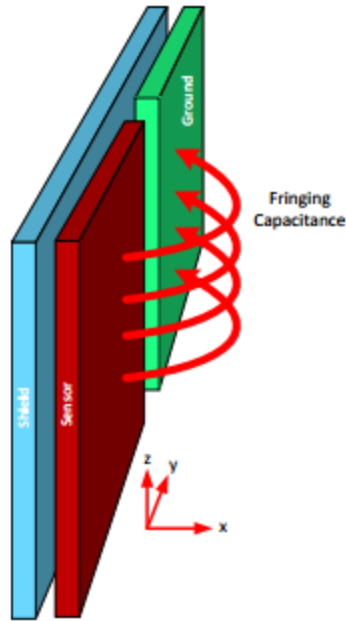
Figure 4.2 Parallel Fingers Topology

The parallel finger topology is often used when the material to be sensed has a large surface area, like water level sensing, moisture, or ice sensing. Additionally, this topology allows for modifications in the setup for a wide directivity along the electrodes. In this thesis, different modifications were made to this topology and a sensitivity test was also performed before the sensors were actually fabricated to be in-corporate with the sensing circuitry.

4.3 Design Considerations

4.3.1 Simulation Software

The choice of simulation software is paramount in any engineering design, because it provides a first insight on the expected result and performance. Furthermore, a well-designed simulation

also provides the result on the effect of design parameters on the results. For this design, COMSOL Multiphysics was selected because it provides an in-depth visual analysis in modelling various engineering problems. This software uses partial differential equations PDEs to compile, solve and provide solutions to complex engineering models [23]. The software has been used in the field of acoustics, fluid dynamics, and Micro Electromechanical systems (MEMs). In comparison with other software like ANSYS which have the same capability, COMSOL does not require an in-depth knowledge of the mathematical or numerical analysis of the models; instead, models are built by simply specifying physical parameters like length, width, temperature and other constrains where need be. The software compiles the PDE of a given models using the defined parameters and subdomain values and provides a well-documented result and compilation statistics. Furthermore, meshes, electrostatics calculations in forms of field volume and field lines can be visually represented in COMSOL which is very useful in electrostatics simulations so as to see where the field lines are most dense.

In this thesis, COMSOL is used to model the capacitive copper tracings on silicon PCB, The same material specifications used in COMSOL was specified for fabrication. Furthermore, ice blocks of different thickness are added to the model to see the change in capacitance and the result is compared alongside the experiment. A sensitivity analysis is also performed by changing the width of the spacing between the sensor plate and the ground plate; this is as a guide in determining the optimum design with the largest electric field fringing lines and the lowest base capacitance.

4.3.2 Choice of sensing material

The material used in the sensing material is very important because not every metal can be used as a sensing electrode, although, the geometry used determines the sensitivity of the sensor; which in turn determines how accurate the sensor can measure the thickness of the target material. For the initial sensor simulation, come material selection criteria are drawn, these criteria includes low cost, easy to manufacture on a PCB, light weight and good tolerance to moisture and rust, and the dielectric difference with that of air.

The dielectric constant of a material is the measure of the materials ability to transmit electric field. Copper on silicon substrate is a good candidate because of the difference in dielectric properties compared with air and water. The best option decided upon at this stage is copper on FR4 Fiberglass substrate. The surface of the PCB might be coated with epoxy with a dielectric constant similar to glass which is 4.5 to 6. Materials used in the simulation were matched with the actual physical material used in the design as documented in this thesis.

4.3.3 Geometry of the Sensor Plate:

Electrode geometry is a very critical design consideration as it determines the direction of the electric field lines as charges migrate from positive to negative electrode creating an electric field cloud. The geometry employed in this thesis is a variant of the parallel finger topology. This was chosen because the fringing electric field from the wider surface area would be best fit to determine ice and water properties.

Figure 4.3 [21] shows central ground geometry, this is ideal for sensing materials with wider surface area, and this setup is required for a high directivity along the width of the electrodes. Furthermore, the plot to the right shows the capacitance measurement on each side of the

charged electrode. As observed, the peak capacitances occur at the sensor ends of the geometry; this is only directive to the materials in either end of the setup.

On the other hand, Figure 4.4 [21] shows the central sensor symmetry, this is a modified alternative of the parallel finger geometry, as the sensor is in between the ground plates, and it provides a sharper response over a small surface area. This alternative is not the best for ice sensing since the sensitivity is required throughout the whole area of the plate.
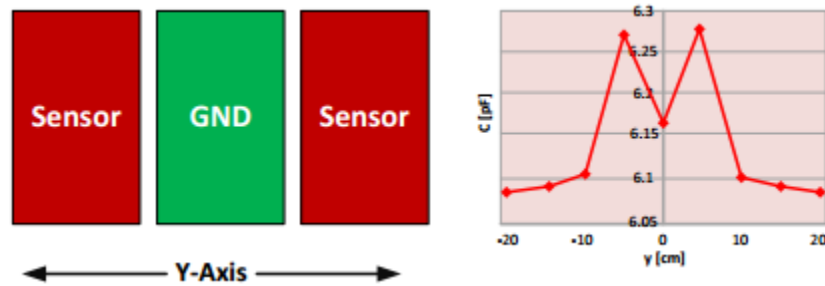
Figure 4.3 Central Ground Symmetry.
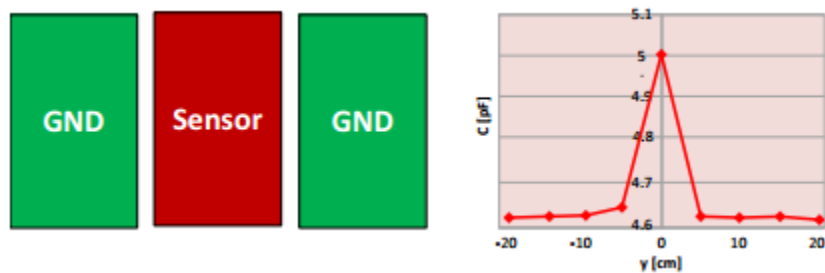
Figure 4.4 Central Sensor Symmetry

After careful consideration of the target material, a combination of the central ground sensor and the central sensor is suggested, the capacitance calculated should be the overall capacitance throughout the entire area of the sensor plate. Hence, a wide and sharp response is simultaneously needed. The revised version of the parallel finger topology will be an interlocking central ground and central sensor hybrid configuration known as the "comb"

topology. This sensor is fundamentally based on the basic principle of material sensing which is a detection technique for anything that is conductive or possess a dielectric constant different from air.
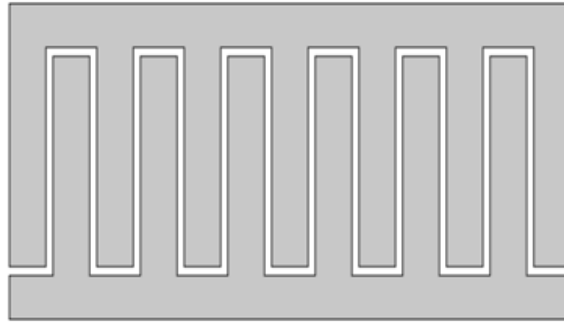
Figure 4.5 2D Comb Sensor Design

Figure 4.5 above is a 2D COMSOL representation of the comb topology, as shown, one end of the comb is interconnected as the GNDed finger and the other end will be the charged or the sensor finger. During the cause of the design, other variations of the comb sensor will be produced and tested, before the final design for the sensor will be established.

4.3.3 Interfacing Capacitance and copper spacing

The front end capacitance as seen by the sensing circuitry is very important in this design because the capacitance to be read will be determined by the circuitry designed, the capacitance range should also be determined. The FDC1004 integrated circuit will be used to transfer charge from the sensing electrodes to the sigma delta analogue to digital converter ADC. The capacitance to digital converter has a capacitance null value limitation of 100pF. Due to the hardware limitation, the overall size and the spacing between the copper tracings become critical

in determining the overall capacitance. The spacing between the copper tracings determines the distribution of the fringing field lines.

Based on preliminary simulation results, a spacing of 0.5 to 1mm is initially considered, as it provides the best combination of large fringing fields with capacitance in Pico Farads. Furthermore, the fringing field lines should be as large as possible to go through a considerable ice thickness, and also provide flexibility for deployment, in case the sensor is to be mounted behind a protective class, the field lines should be large enough to accommodate the glass.

Hence, an ideal sensor layout for ice thickness detection should be one that produces the farthest extended electric field fringing lines which reaches the overall area of the sensor plate with minimum capacitance to suite the FDC1004.

4.3.4 Effect of parasitic capacitance

Some parasitic capacitances are introduced into this system by all non- guarded electrodes; this is made of little effect by the spacing between the copper sensor and round sensor is kept small enough to null the effect. However, the most important capacitance to consider is the external practice capacitance resulting from the connecting copper wires. The electronics of this sensor cannot distinguish the parasitic capacitance from the base capacitance since they are all connected in parallel. Hence for this design a guarded electrode and adequate shielding is used outside the electrode structure. Toth and Meijer [24] in their research on have shown that the capacitance between the connecting wires can easily be reduced to about 20 aF by simply using a shielded coaxial cables to connect the electrodes to the circuitry; the final length of the connecting wires are advised to be as short as possible. In critical cases, a series dead capacitance

bank can be installed in series with the capacitive plate to reduce the capacitance to the desired range.

4.4 Prototype Descriptions and Simulation Results

4.4.1 First Prototype

The first capacitive sensor tracing is designed in Cadsoft Eagle PCB design then extruded in 3D geometry in COMSOL to perform the capacitance simulation. The initial conception was a simple interlocking copper tracing which area small enough to get the desired capacitance range. The purpose of the initial design is to get an in-depth look at the output capacitance and tune the geometry to suite the design.

Table 1 Design Parameters and Results for prototype 1

Trace Parameters	Measurements
Copper tracing spacing	1mm
Copper tracing length	32mm
Copper tracing Area	800mm^2
Copper tracing width	2mm
Simulated base capacitance	11.25pF
Measured base capacitance	22.45pF
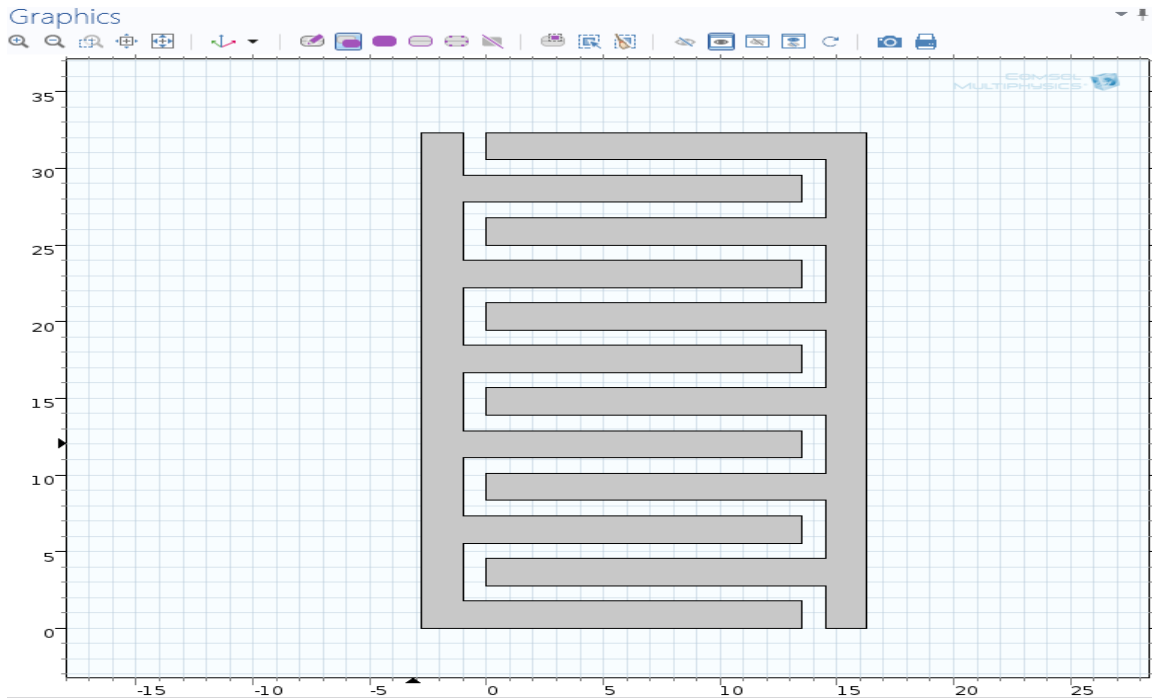
Figure 4.6 2D COMSOL drawing of Prototype 1

The first prototype was used in theory as an initial stage of the sensor design to obtain suitable design parameter. A second prototype is then proposed to reduce the base capacitance to at least 10pF; this will give more room for calibration. Also, this design showed some inconsistency in calculated capacitance when the file is ran in COMSOL. These problems are staged to be addressed in the second prototype.

4.4.2 Second Prototype

The second prototype is designed directly in COMSOL 2D module and extruded in 3D unlike the first that is designed in Eagle PCB design software. This is to address the problem of inconsistencies in measurement which could have come from importing the CAD file into COMSOL.

Figure 4.7 below shows the COMSOL simulation of the second prototype, this features a longer trace length, but the trace width is unchanged, hence has a longer sensing area (Area between the sensor tracing and the ground tracing). This design is used to show the change in base capacitance with change in basic parameters.
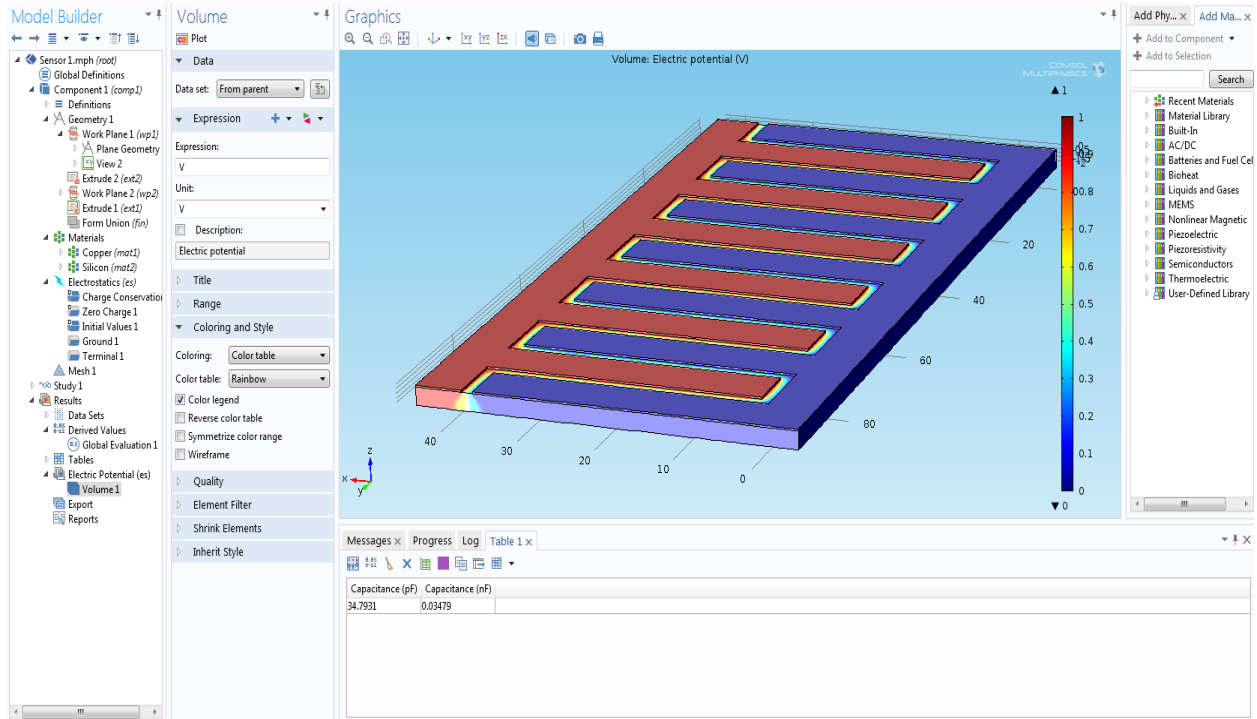
Figure 4.7 3D COMSOL Representation of Prototype 2

The Figure 4.7 above shows a base capacitance of 34.79pF which is again higher than expected, as the base capacitance need to be small enough to allow calibration.

Since the aim of this thesis is to provide an in-depth analysis of designing a capacitive based sensor for marine icing, this means that at warmer temperature, the sensor could simply be exposed to just water without any freezing. Hence, further analysis was performed on this prototype to show the change in capacitance in the presence of a 1mm water film. In Figure 4.8 below, a 1mm water film is added as a material available in COMSOL, the copper tracings are

insulated to eliminate conductivity in the coupling impedance. Hence, the light epoxy film is included in the simulation mole between the copper electrode and ice.
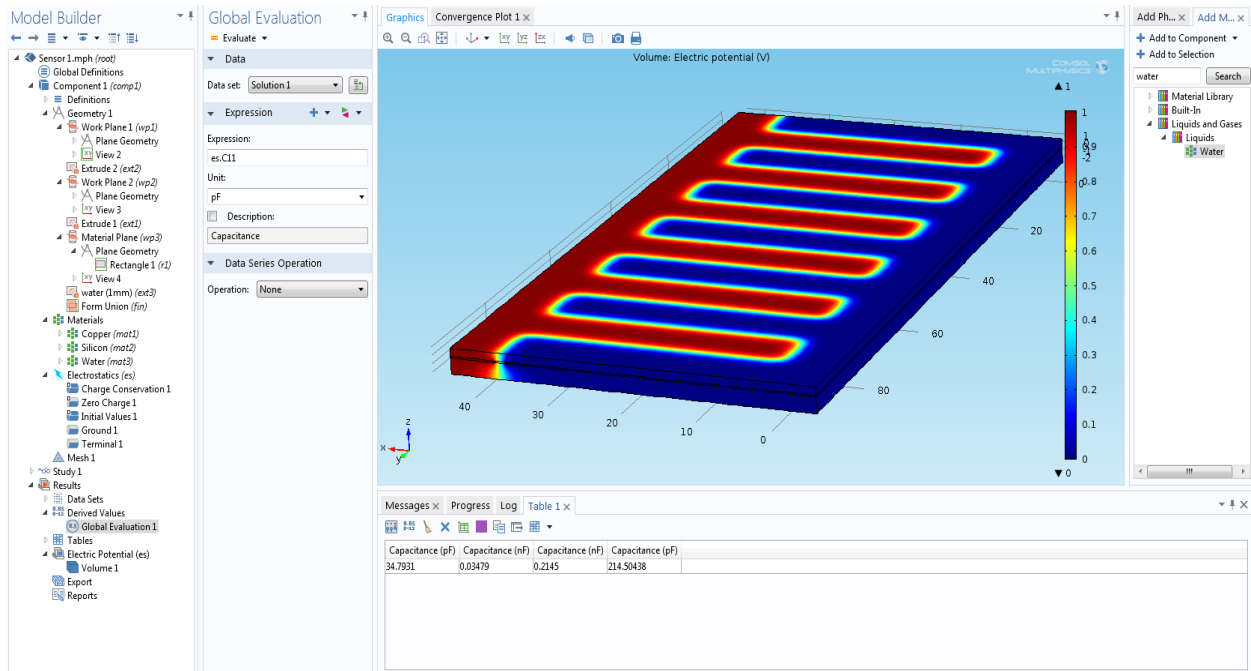
Figure 4.8 COMSOL simulation of sensor tracing with 1mm water film

The relative permittivity of water at about 0^oC is about 88 as used in the simulation. As expected from the simulation above, the simulated capacitance is 214pF and the measured capacitance using the LCR meter is 250pF.

Next, several ice simulations is performed to see the change in capacitance with ice thickness. Figure 4.9 and 4.10 shows a COMSOL simulation using 2mm ice thickness on the sensor plate. Figure 4.11 is a plot to show other results from various ice thicknesses.
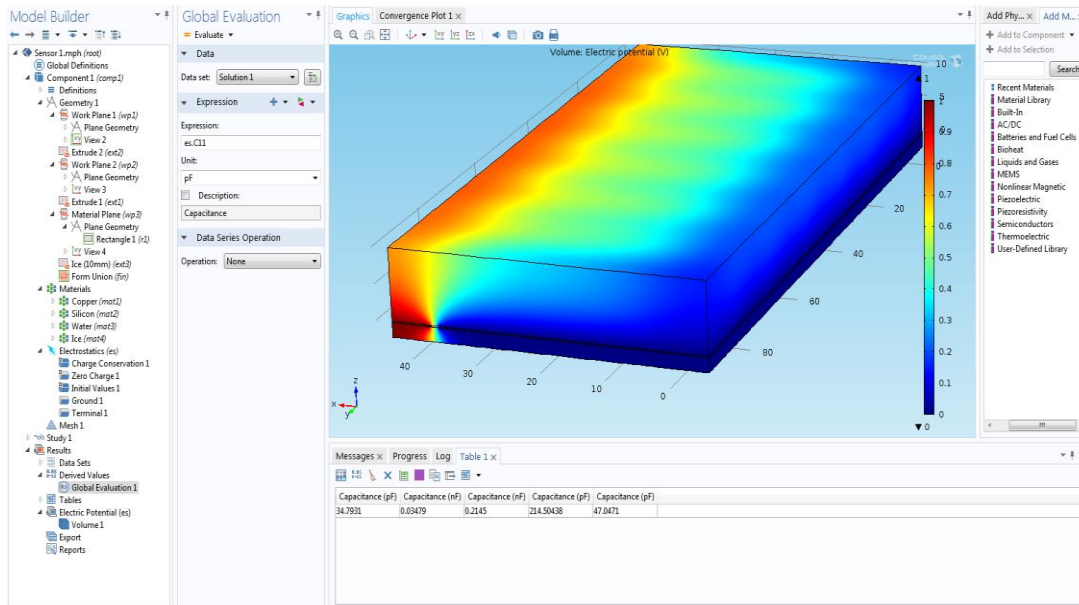
Figure 4.9 COMSOL Simulation for change in capacitance due to 10mm icing
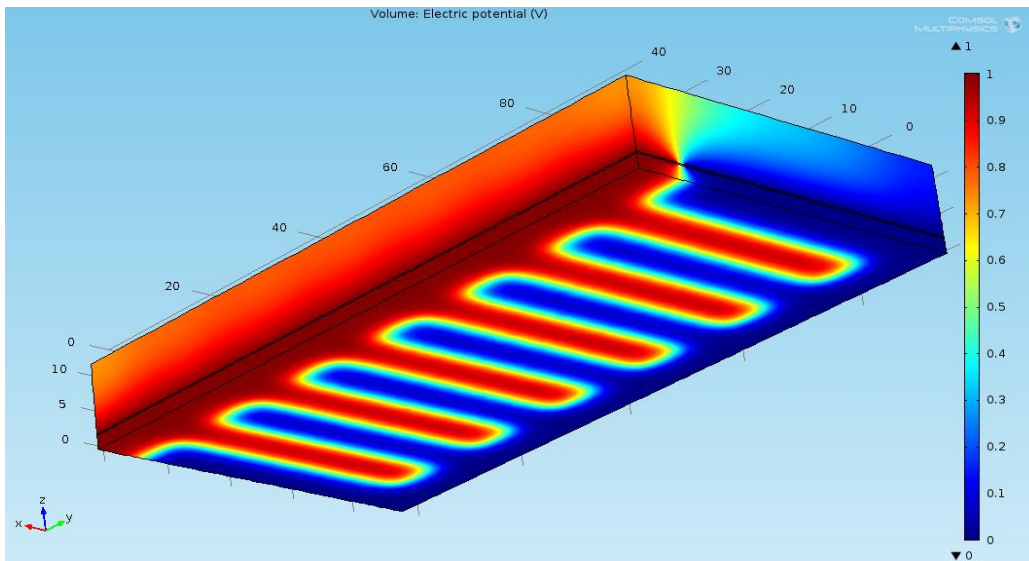
Figure 4.10 Bottom view of the electric field effect through silicon substrate

The above analysis shows some consistency with the expected results, for 10mm ice the capacitance is about 47pF.
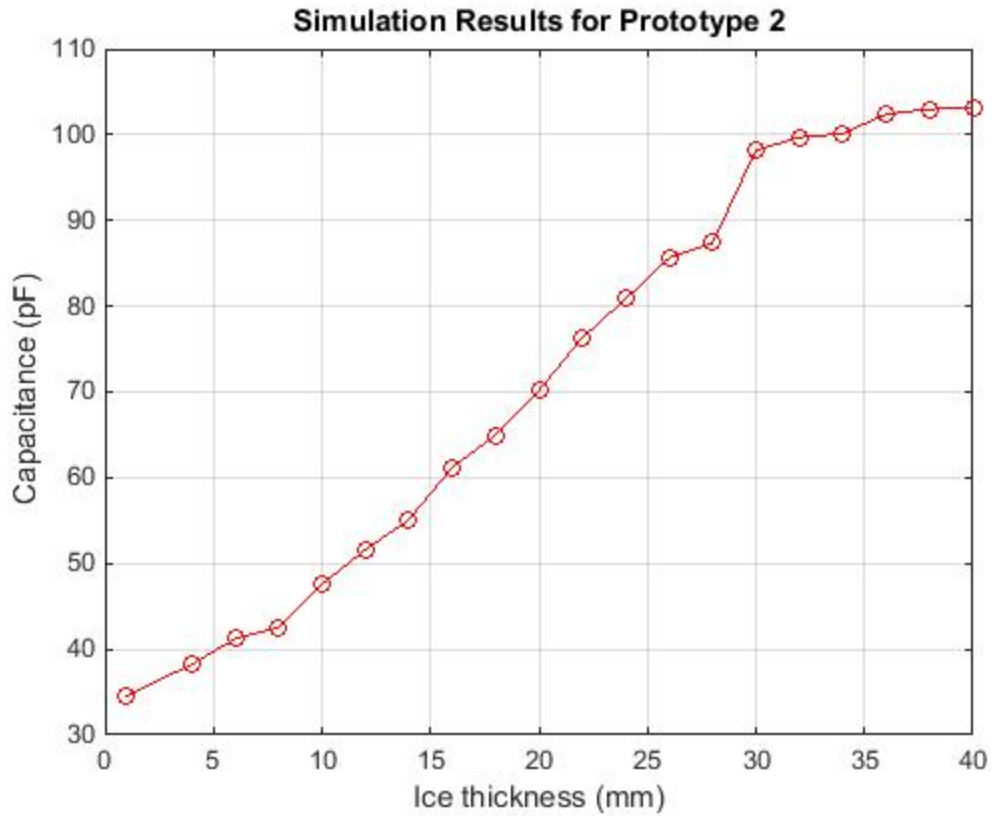
Figure 4.11 Simulation results for capacitance vs Ice thickness for prototype 2

A sensitivity analysis is performed to verify results obtained in Figure 4.11. For this analysis the fringing field lines are plotted and observed, lesser field lines penetrate the ice with increase in ice thickness, in other words, this sensor is more sensitive to measure ice thickness between 0 to 30mm with some accuracy.
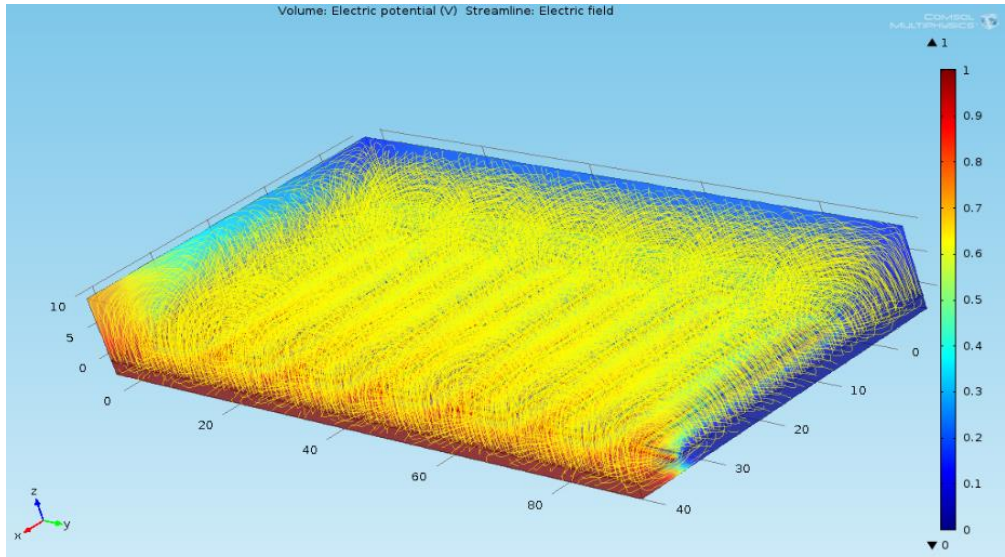
Figure 4.12 Sensitivity Analysis showing fringing field lines

This prototype design is fabricated and measured using an LCR meter the Figure 4.12 above shows the fabricated sensor tracing on PCB with the following parameters.

Table 2 Design Parameters and Results for Prototype 2

Trace Parameters	Measurements
Copper tracing spacing	1mm
Copper tracing length	35mm
Copper tracing Area	835mm^2
Copper tracing width	2mm
Simulated base capacitance	34.79pF
Measured base capacitance	36.25pF
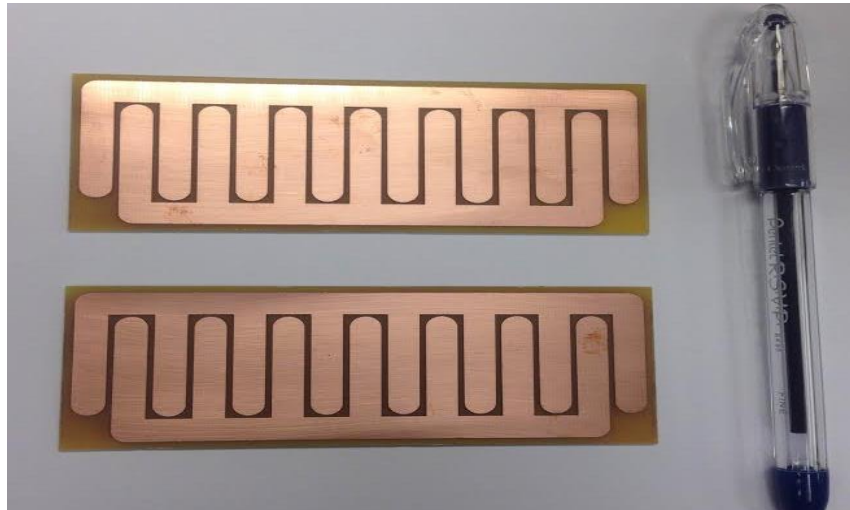
Figure 4.13 Fabricated prototype 2

The problem with this design is that the output base capacitance exceeds expected values; this is needed to be as low as possible to give to provide room for calibration up to 100pF which is the ADC requirement. Furthermore, this prototype is fabricated with regular PCB copper cladding on Fiberglas substrate, an inconsistent result was obtained when tested with ice. This observation was never seen in the simulation stage, perhaps substrate material absorbed some moisture which added to its instability. Hence, the following sensor prototype is desired to find a solution to these short comings.

4.4.3 Third Prototype

The third prototype was initiated to address the base capacitance issue, as well as to obtain an improved sensitivity.

Figure 4.14 below shows the COMSOL simulation of the third prototype, the length of the sensor was reduced by one third and the width halved. The sensor gap is kept the same effectively to see the changes in the capacitance with a reduced area.
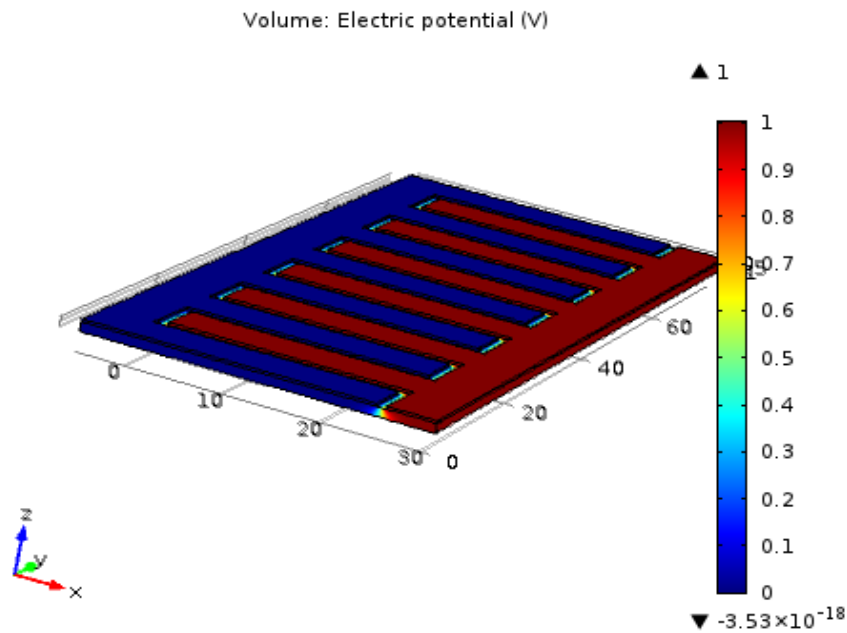
Figure 4.14 3D COMSOL Representation of Prototype 3

The third prototype showed a base capacitance of 14pF. The capacitance of the fabricated prototype as show in Figure4.14 measured 13.35pF. This is much lower as expected and provides enough room for calibration.

Next step is to provide further analysis for to observe the change in capacitance in the presence of icing on the surface. A 1mm water film is added as a material available in COMSOL, Figure 4.15
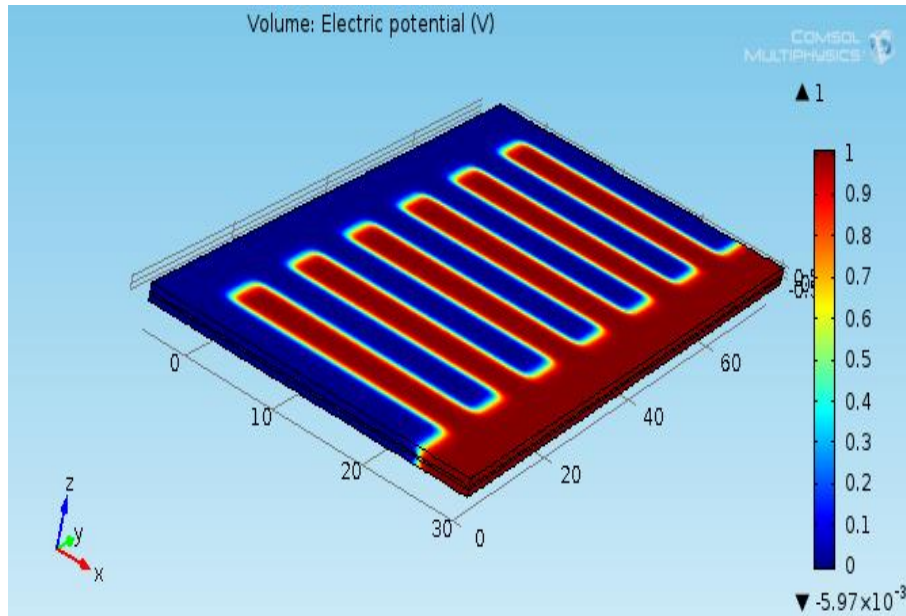
Figure 4.15 COMSOL simulation of sensor tracing with 1mm water film

As expected, a spike in capacitance was obtained because the relative permittivity of water is about 88 times more than that of air, hence for a1mm water film, a base capacitance of 71pF is observed and a measured capacitance of 68pF using the LCR meter after spraying the surface with a simple spray bottle.

Next, an ice simulation is performed to see the chance in capacitance with ice thickness. Figure 4.16 shows a COMSOL simulation using 2 mm ice thickness on the sensor plate. Figure 4.17 is a plot to show other results from various ice thicknesses.

From the simulation, a base capacitance of 23.83pF was obtained and a measured base capacitance of 35pF. This result shows some consistency with the expected values because the relative permittivity of ice at -20°C is about 3.5. In this analysis, the results show some acceptable consistency.
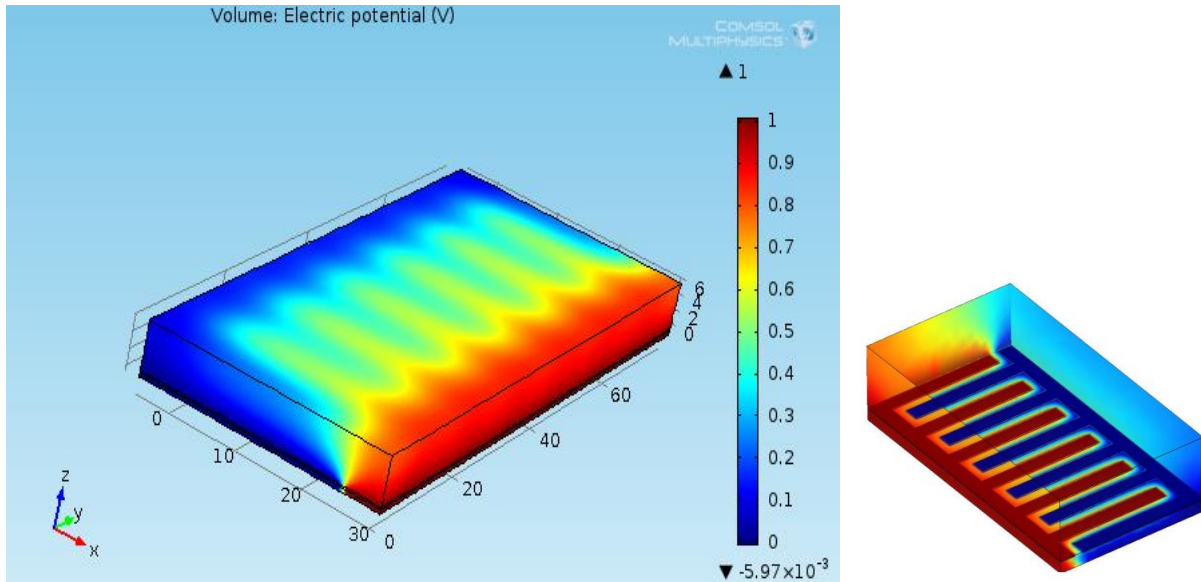
Figure 4.16 COMSOL Simulation for change in capacitance due to 10mm icing

To obtain some more valuable results, various ice thicknesses were simulated and observed in comparison with the previous prototype, the aim was to obtain high sensitivity and low base capacitance.
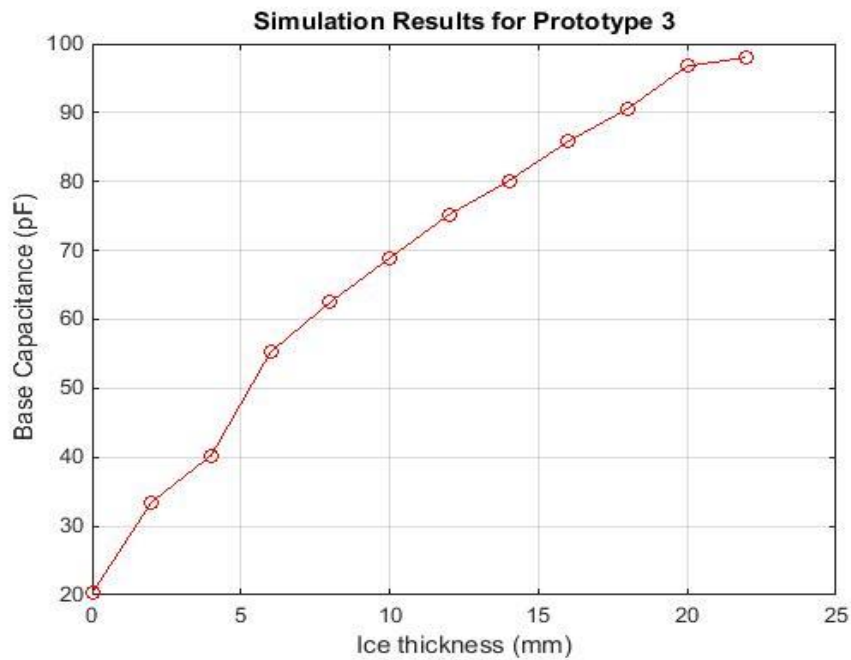
Figure 4.17 Simulation results for capacitance vs Ice thickness for prototype 2

The above results show that the prototype could only measure ice thickness up to 30mm and the graph flattens out at about 90pF. Further simulation work is done to produce a visual fringing field representation of the prototype. Figure 4.18 confirms this; as observed, the field lines are denser below 25mm range.
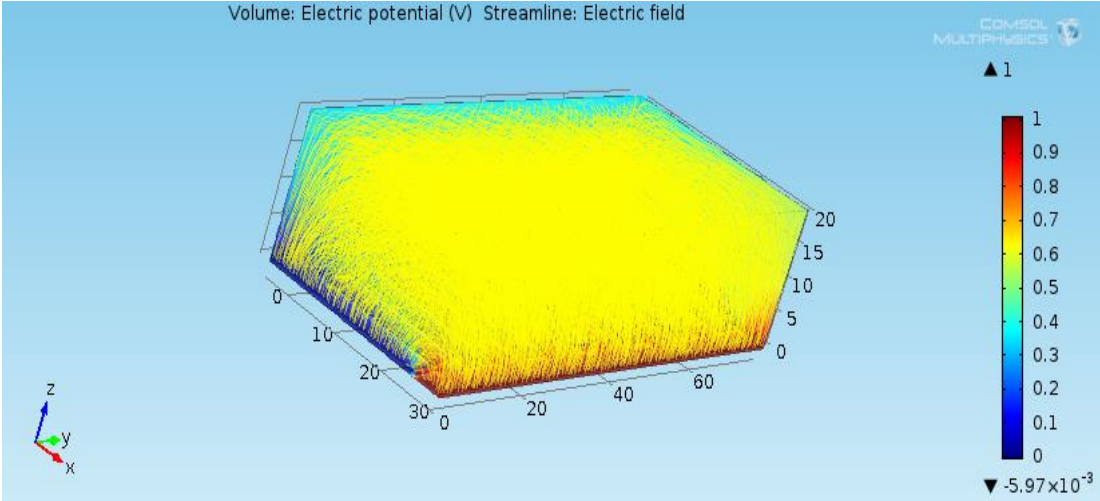
Figure 4.18 Sensitivity Analysis showing fringing field lines

This prototype was fabricated based on the following material specifications.

After careful considerations, the copper tracings will have the following materials specifications.

- FR4 (fibre glass substrate)1.5mm standard 1 Oz Cu

- Single sided (top copper only)

Figure 4.19 Fabricated prototype 3

The prototype was also tested, and the results were promising, longer electric field lines were obtained, and the results of the simulation closely match the measured capacitance and the results of the preliminary ice test. Figure 4.19 shows the backside of the PCB embedded in clear caulking just to provide additional surface for an even ice accretion surface. At this stage, the results were satisfying, but there was a need to try modifying the sensor geometry to investigate a change in the direction of the fringing field, which could provide an improvement in the overall ice sensing capability.

4.4.4 Forth Prototype

Although there is no need for another prototype design, the effect of a fringing filed in a circular coordinate is needed to be investigated for a complete engineering design approach. Figure 4.20 shows the fourth prototype is constructed in solid works instead of Eagle. This was because it involved a complicated combination of curved lines which could not be done in electronics software like CadSoft Eagle or Kicard.
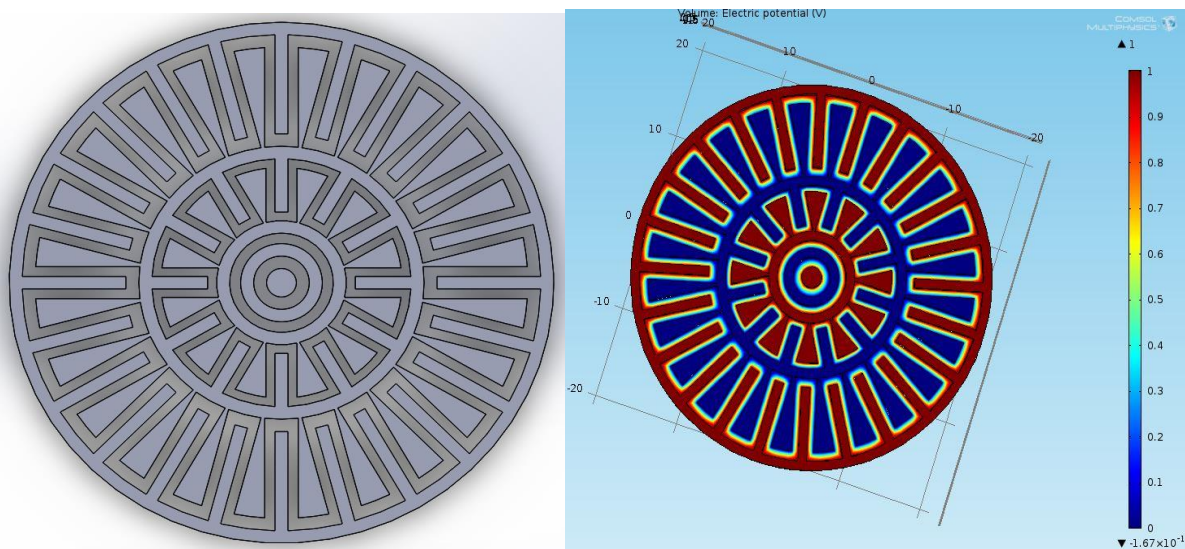
Figure 4.20 3D COMSOL Representation of Prototype 4

Figure 4.21 Fabricated prototype 3 Sensor Plate

Similar to the other prototypes, the red electrode is the terminal and the blue electrodes are the grounds. The individual electrodes are interconnected in the PCB bottom layer. The final prototype shown above is a combination of the interlocking combs fingers and a sequence of alternating sensor and ground electrodes. The geometry was changed to create a circular fringing field at the edge, and produced a stronger fringing and longer fields. Although, The this prototype measured a base capacitance of 20.45pF which was slightly higher than expected that could measure ice thickens of up to 40mm as seen in Figure 4.21.

The specifications are:

- 4.58cm X 5.58cm.

- FR4 1mm standard 1oz Cu.

- Single sided copper tracing.

- Fused 63/37 SnPb finish.

- Green photo Imageable solder mask.

Further ice and water simulations were performed as the other sensors; the prototype could sense water film with a base capacitance of 75pF. The Figure 4.22 below shows the CAD drawing of the final sensor.
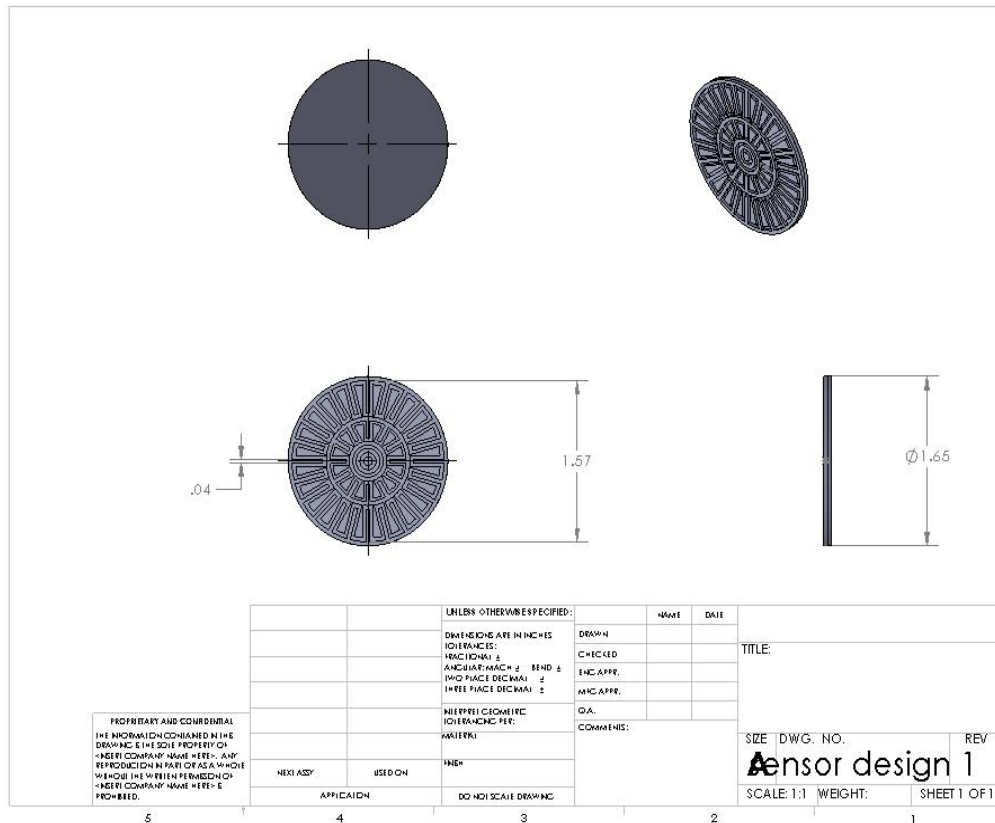
Figure 4.22 Final Drawing for Prototype 4

Figure 4.23 shows the result of the ice simulation on COMSOL, it is observed that the change in geometry and shape of the sensor have significantly improved the sensitively and the sensing range. This is because the alternating sensor and ground electrodes provides a more diverse path for the fringing fields. Unfortunately, testing the sensor with real ice experiment proved that the

sensor was unable to measure ice accretion more than 5mm as proposed by the design simulation. This was because the electrode spacing and orientation was too tightly meshed together than the electric field lines became shortened.
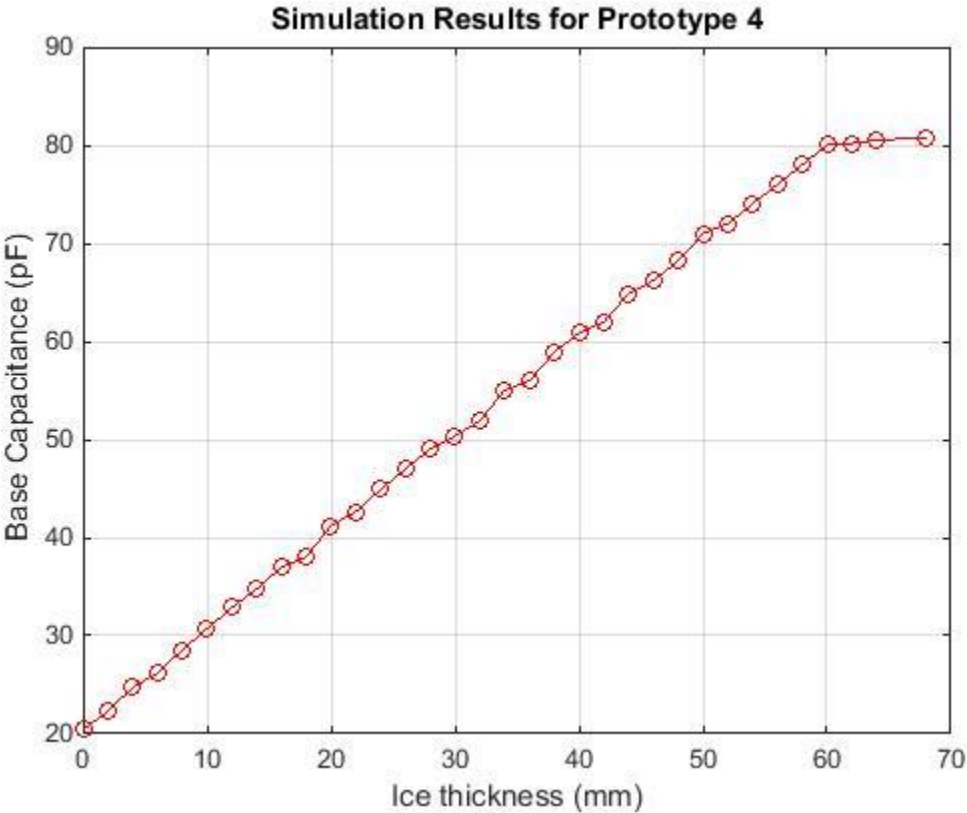
Figure 4.23 Simulation results for capacitance vs Ice thickness for prototype 4

4.5 Design Conclusion

Based on the simulations and results the prototype 3 seems to be the best option for the marine ice sensor because it provides a more reliable and consistent result, and could also detect ice thickness for up to 30mm. Pending to actual controlled experiment, this sensor plate is fabricated on a PCB based on the actual specification described in the previous section.

Chapter 5

Sensor Electronics

5.0 Introduction

The function of the sensor electronics is to convert the information obtained from the sensor tracing to more useful information. This marine icing sensor setup contains many other accompanying electronics, as described in the following section.

The block diagram shown in Figure 5.1 is the setup for the whole sensing system
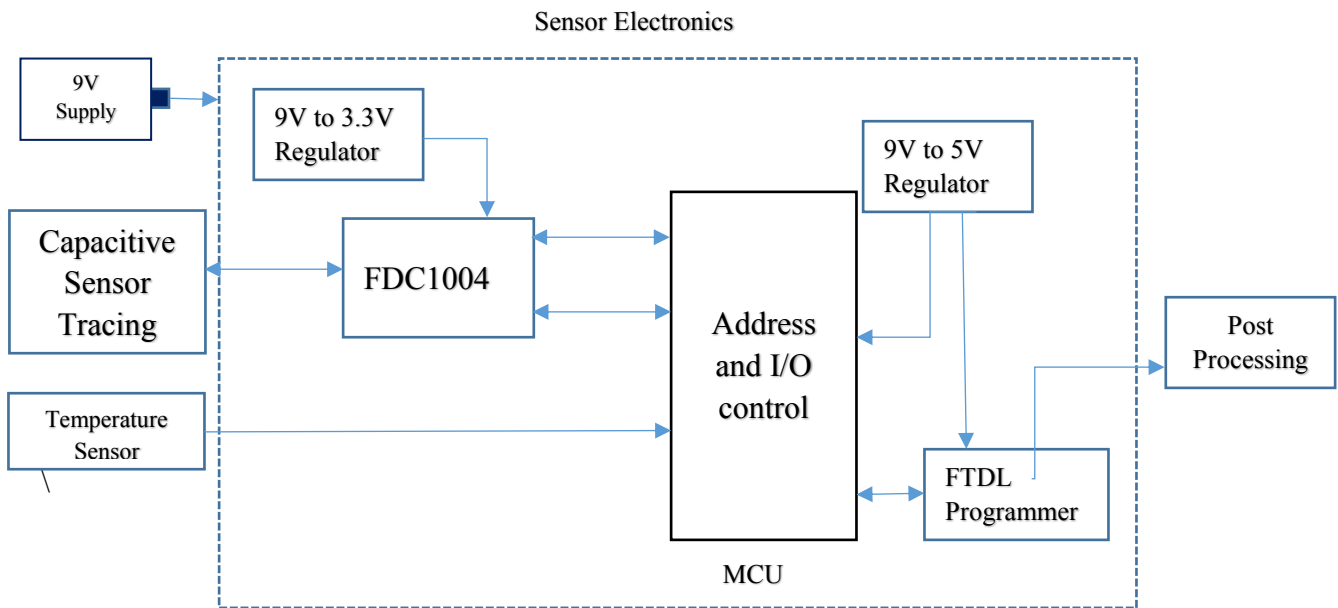
Figure 5.1 Block diagram showing sensor electronics

5.1 Capacitance to Digital Conversion

There are several techniques used to measure capacitance, however for marine icing application there is a need for a reasonably good and reliable measurement. Consequently, there are some trade-offs in achieving these criteria. For example, in most cases the sensor capacitance is designed to be very low, in order of a few pF; and often, the parasitic capacitance is more or comparable in value to the actual sensor capacitance.

From the previous section, it can be observed that complete shieling of the capacitive sensors are not always possible, hence, proper base masking and short shielded wires are used.

Baxter et al [18], in his publication presented two main techniques for capacitance to digital conversion.

- Excitation and A-D conversion
- Circuit and system level technique

The measuring sensors are required to be very low in a few pF, the excitation and A-D conversion becomes the better technique to measure capacitance with little effect from the parasitic capacitance. To measure a sensor capacitance, the terminal end of the capacitor need to be current excited. The excitation waveform is not really important some applications have used sine wave or square wave with some success. However, sine waves excitation measurement could show high resolution without meeting the requirement of cost and power minimization [18]. Hence, this thesis will employ a capacitance measurement based on square wave excitation using A/D sigma-delta conversion.

This principle have been used in modern chips like AD7745, AD7746, AD7747 and AD7150 produced by Analog devices, and also seen in FDC1004, FDC2112 manufactured by Texas instrument.

The capacitance to digital converter is a modified version of a voltage to digital converter. Figure 5.2 [24], shows the working principle of the CDC. The digitization is established when the comparator output is zero (low), the charge transfer from the C_xV_{ref} is transferred to C_{int}, and when the comparator output goes high, the charge $(C_x - C_{ref})\ V_{ref}$ is transferred to C_{int}. As a result of balance of charge, the stream of zeros and ones appears on the output of the comparator, the ratio of the number of clock cycles equals $C_x\ /\ C_{ref}$ [25]. The decimation filtering is then performed on the output and digital capacitance can be obtained.
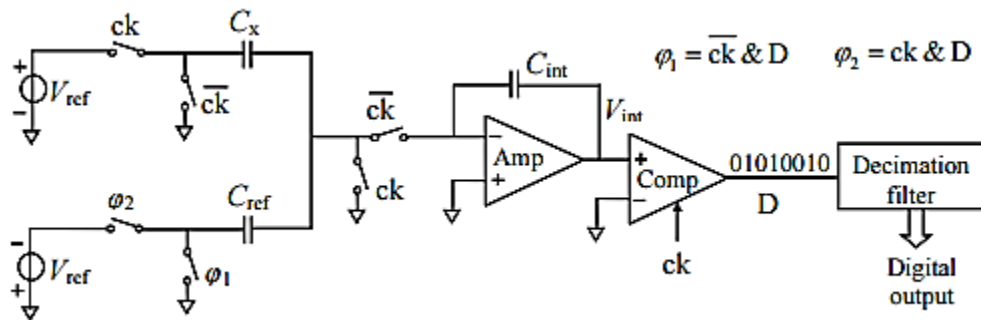
Figure 5.2 Capacitance to Digital Conversion using Sigma-delta

5.1.1 FDC1004 Capacitance to Digital Converter.

This thesis will explore the sigma delta conversion method found in the FDC1004 manufactured by Texas instrument. The FDC1004 technology implements a switch capacitor circuit to transfer charges from the sensor electrodes to the sigma-delta analog to digital converter [21]. As decided

in section 5.0, the circuit will be excited by a 25 kHz square wave form and after a certain time duration, the charge is transferred into a sample and hold circuit as shown in the Figure 5.3 below.
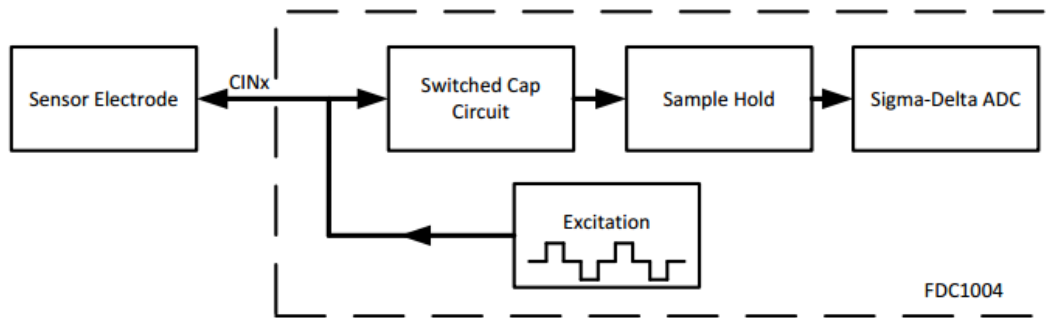
Figure 5.3 FDC 1004 theory of operation

5.1.2 ATmega328P Microcontroller

There is a need for a microcontroller to control the FDC1004 and the temperature sensor. The microcontroller also converts the capacitance to show the ice thickness at that a certain time. The ATmega328P was selected for this thesis because it is readily available high performance, low power, and 8-bit microcontroller, easily programmable in C language and can run off a 5V power supply available on the board. The ATmega328P also allows for I2C interfacing of the FDC1004 through the SDA and SDL available on chip. It is also responsible for the 1-wire interfacing of the temperature sensor. Details on the connection are shown in the schematic drawings in Figure 5.2.

5.2 DS18b20 Temperature Sensor.

A DS18b20 is used to log the temperature during ice accretion. The DS18B20 digital thermometer provides 9-bit to 12-bit Celsius temperature measurements, as shown in the block diagram in Figure 5.4 [21]. The 1-wire communication standard as designed by Dallas semiconductor is a convenient way of transferring from the microprocessor power and data through a single wire. The DS18b20 will be exposed to extreme temperature hence; it was chosen because of the following reasons.

- Capable of Measuring Temperatures from -55°C to +125°C (-67°F to +257°F)

- Measurement accuracy of ±0.5°C from -10°C to +85°C

- Programmable Resolution from 9 Bits to 12 Bits.
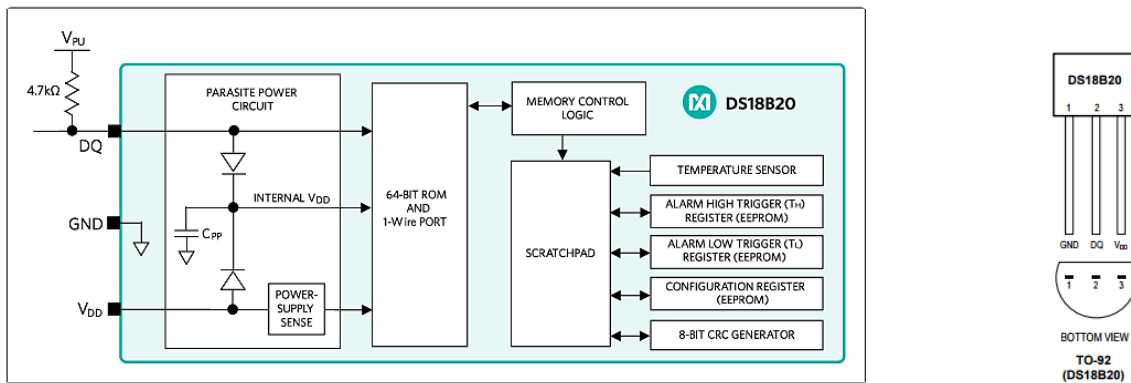
Figure 5.4 Block Diagram of the DS18b20 and Pin-outs

Chapter 6

Final System Design

6.0 Introduction

The full system is built on a prototype board as shown in Figure 6.1. The system is powered from a 9V battery source and converted to a 5V and 3.3V as needed. The system is designed to operate with power coming from either the FTDL cable or the 9V battery but not simultaneously, so as to give adequate flexibility if system expansion is needed.
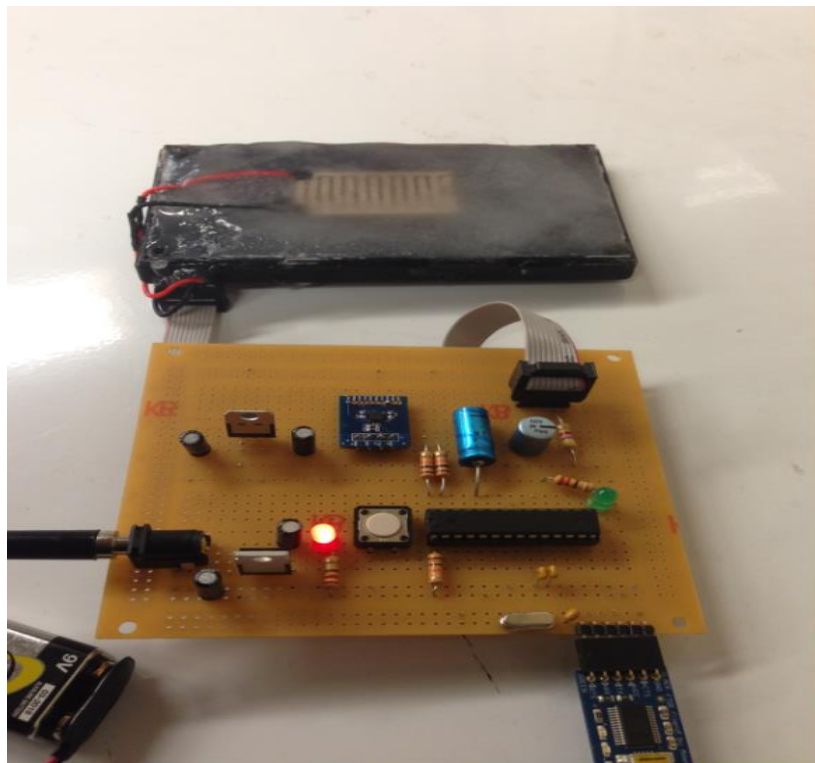
Figure 6.1 Full System Prototype

As shown in Figure 6.1, An FTDL cable is used to program the micro controller and also used to output data from the system for post processing. This system is also designed with connection pins in case an LCD screen is needed instead of viewing the results on a computer screen.

6.1 System Schematics.

The system schematic is shown in Figure 6.1 this is designed in KiCard a free PCB design software and could be used as an effective tool to view and to convert this sensor electronics to a PCB should it be needed in the future. The FTDL is shown in the schematics as it was a separate hardware on its own. The sensor plates are also not shown in the schematics, as there was no way to incorporate them. The sensor plates will be connected to the CIN1 and GND as shown.
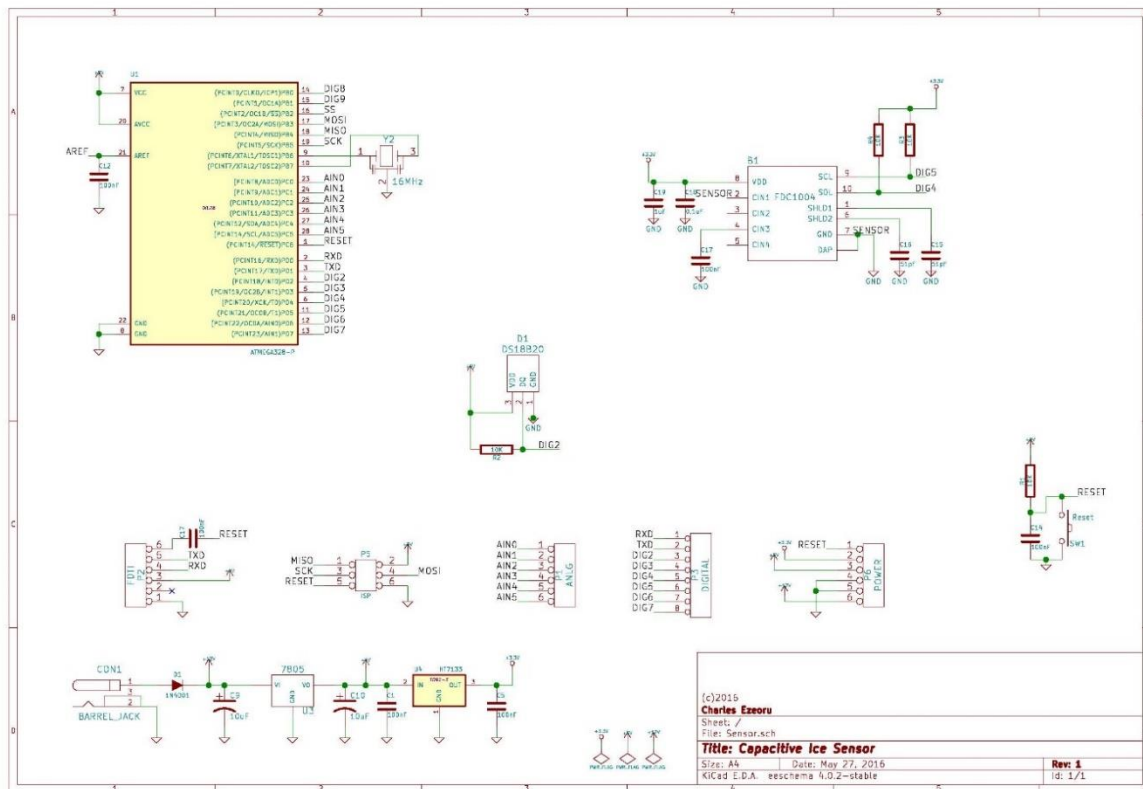
Figure 6.2 Overall system Schematic

6.2 Programming, System Interface and Testing.

6.2.1 The I^{2}C Interface

Some of the most important programming lines are listed here and explained for clarity, APPENDIX A contains the full code and header files used in this thesis.

 # include <Wire.h>: This is used to initiate the 12C capability

 # include <FDC1004.h>: Header file for the FDC1004

Wire.begin ()>: Initiate the Wire library and join the I2C bus as a master or slave

Wire.beginTransmission: This is used to start transmission the 12C slave

Wire.endTransmission: This is used to end transmission the 12C slave

Write (): Used to queue bytes for transmission to the master device

NOTE: The FDC1004.h header file handles the serial interfacing with the FTDL cable used for programming.

In this setup, the ATMega328P connects to and configures the FDC1004 Capacitive Sensing chip over I2C. For this sensor, the FDC1004 is configured in a single end mode as shown in Figure 6.2, the single end mode compares the capacitance value to an established ground within the FDC1004. The ATMega328P reads the capacitance output from the IC as a 4 bytes data, digitally outputs it to the transmitter.
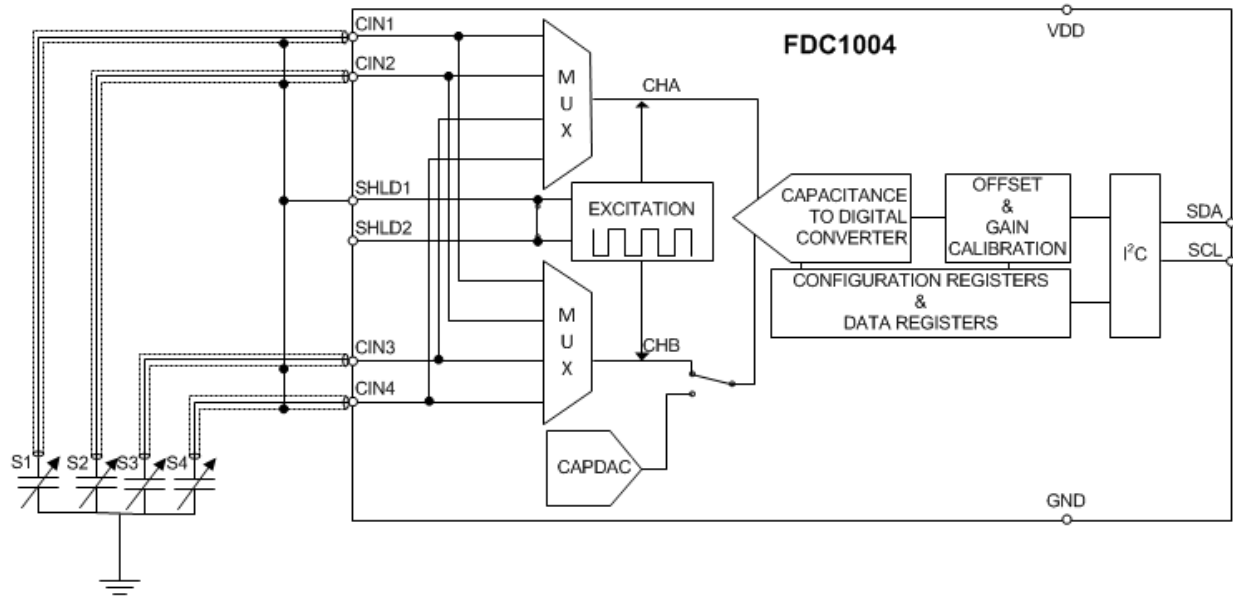
Figure 6.3 Single-Ended Configuration with CAPDAC enabled

The Microcontroller connects to the address 0x50 on the FDC1004 and writes to pointer 0xFF
[21]. The microcontroller verifies the connection by reading the device identification 0x1004;
additionally, the microcontroller configures the capacitance measurement register by writing
0x1C00 to the pointer 0x08 enabling the measurement of capacitance input in CN1. This also
triggers one sample of the capacitance, essentially begins the system write functionality. The
FDC1004 runs in normal mode by default with the initial configuration register at 0x0C at a rate
of 100S/s for all enabled measurements. The only enabled measurement for this design is the
CN1 for a single-Ended mode. Next, the microcontroller reads the FDC1004 configuration to
check for measurement completion, and then reads the registers at 0x00 and 0x01 for the MSB
and LSB respectively.

6.2.2 FDC1004 Testing.

The FDC1004 is interfaced with the microcontroller and tested to determine what frequency has the most accurate capacitance reading and the amount of delays needed while sampling. It is important to note that the sampling rate simply measures frequency at which the data is obtained. The FDC1004 hardware has the flexibility to program the output operate in 100 Hz, 200Hz or 400Hz. From the tests, the FDC1004 reads the capacitance with good accuracy, this test was performed using a standard ceramic capacitor 27pF and capacitance readings were taking for over a period of one minute. Figure 6.4 shows some spikes when either legs of the capacitor is touched with the bare fingers, and it returns to the base capacitance shortly. As observed, the sampling rate did not affect the accuracy of the capacitance reading; hence the code is set to 16 samples per second at 200Hz. The test capacitor is connected to the CIN1 and the ground PIN of the FDC1004 and the GND Pin is grounded to the circuit as shown in Figure 6.2.
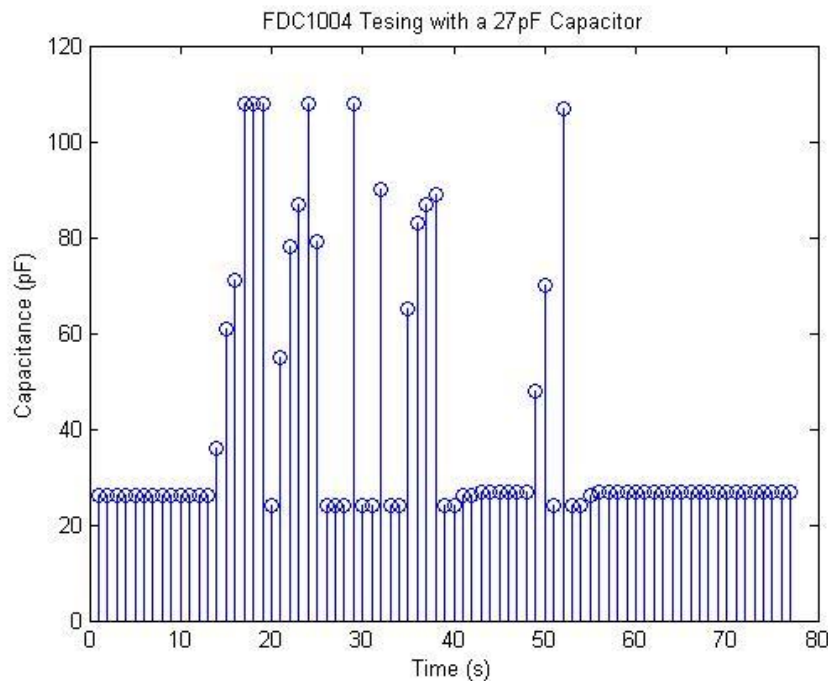
Figure 6.4 FDC1004 Testing Result

Chapter 7

Experiments

7.0 Experiment Setup

The entire experiment is conducted in the laboratory, the system is tested in a deep freezer maintained at -20°C. The sensor plate is placed horizontally in the refrigerator to allow a steady ice build-up on the surface. Figure 7.1 shows the overall set-up in the laboratory and the sensor circuitry and the sensing surface is connected with a short 28 gauge padded data wires. This is eliminates any capacitive interference from the human hands during experiments. Data is collected on a real time python based data acquisition program running on the attached computer via a RSD232 based FTDI connection.
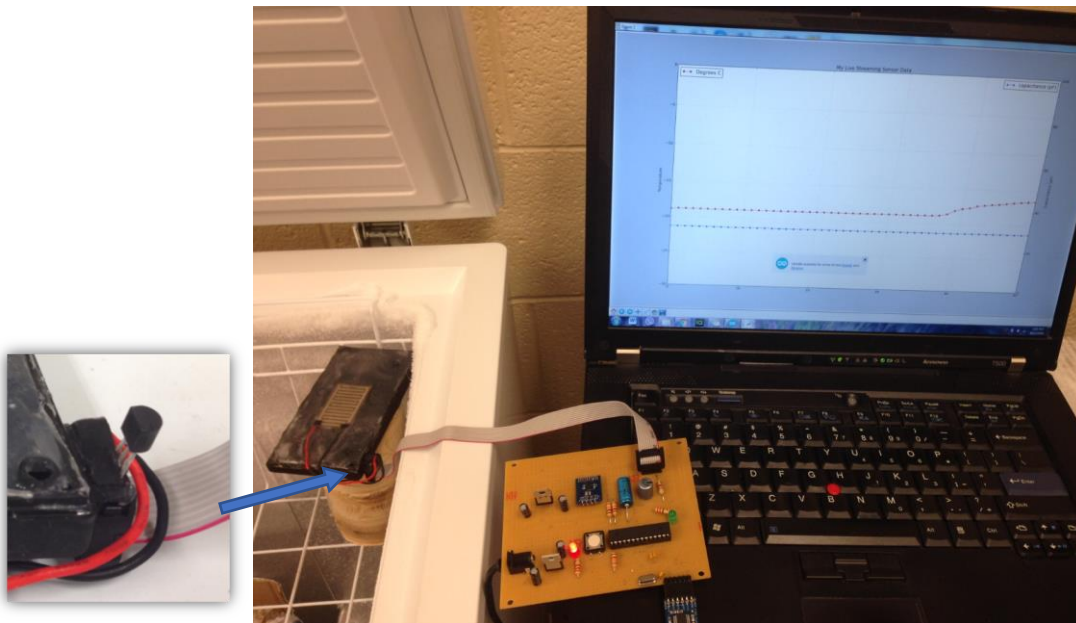
Figure 7.1 Experimental Setup showing the temperature sensor

The icing surface model was obtained using a flat plastic completely covered in clear silicon caulking. The capacitive sensing surface is placed flush with the icing surface mode. This is icing surface model measures 13.2cm by 7.4cm, and 1cm thickness. As shown in Figure 7.1.

7.1 Experimental Methods

The experimental method used in this thesis is primarily to obtain a steady ice growth on the capacitive surface. In this test, the sensor plate is placed in the deep freezer and allowed to reach a temperature of -18.78°C (as measured by the temperature sensor); this is the lowest possible temperature the deep freezer can attain. The active temperature is logged using the DS18B20 attached to the sensor plate. As the temperature plate reaches the expected temperature, tap water of about 5°C is sprayed on the surface of the sensor plate using a spray bottle; this is to obtain a homogenous 1mm water film on the surface. The whole setup is designed at a stable condition and allowed to sit for a very long time until the original temperature of the freezer is reached. The experiment is closely observed until there is no change in the capacitance and the set point temperature of the freezer is reached, the ice thickness of the setup is obtained by

$$Thickness(mm) = \frac{Weight\ Difference\ (g)}{Area\ (cm2)*\rho ice(g/cm3)} \qquad (7\text{-}1)$$

Where $\rho ice = 0.916 g/cm^3$

More water is sprayed on the surface to apply a steady ice buildup as seen in Figure 7.2 for an approx. 2.1mm ice thickness. The real time data is observed through the data acquisition system. This whole experiment is repeated three times in order to investigate the repeatability of the data.

The same experimental methods were applied in salt water experiments as documented in the next section.

Figure 7.2 Ice thickness using fresh water (2.1mm)

7.2 Experimental Results

7.2.1 Ice accretion results using fresh water

The results of the experiment from the data acquisition is shown in Figure 7.3 using fresh water, As observed, the spikes in capacitance as seen on the graph shows the presence of water on the sensing surface, because the relative permittivity of water (70-80) is much higher than air. As freezing occurs, the water changes to solid ice and assumes the relative permittivity of ice (~3.2),

higher than air. The presence of the ice cover creates the dielectric padding which increases the overall capacitance obtained for each stage of the experiment.
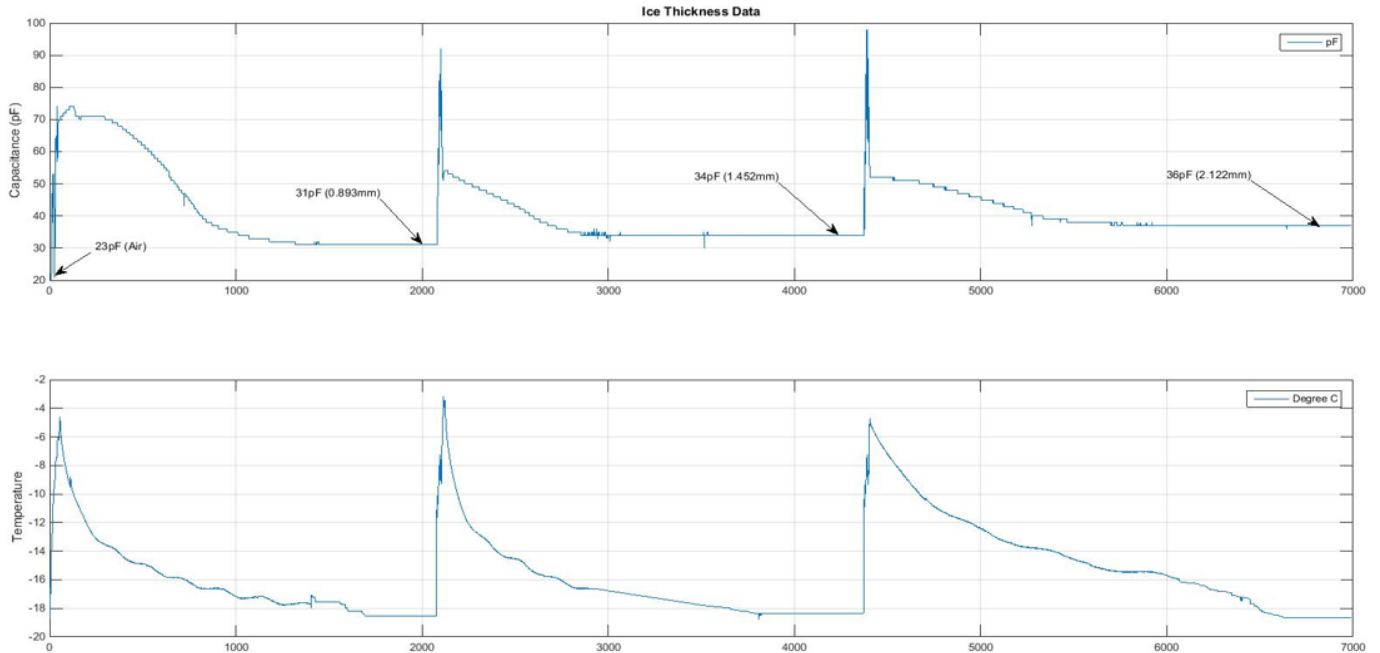
Figure 7.3 Data processing output for ice accretion experiment using fresh water

Further experiments for ice thickness more than 4mm are performed using pre-made ice slabs. The ice slabs are designed with the same container and left to freeze for many hours, until the desired ice sample is obtained. Figure 7.4 shows an experimental setup for an approx. 20.5mm ice thickness using fresh water. Again, the method of the experiment remain the same, the whole sensor plate is brought to the freezer steady temperature of -18.78°C, and this is to avoid excessive melting between the boundary of the ice slab and the sensor plate. The ice slab is placed on the sensor plate and the whole setup is placed horizontally into the freezer and monitored until there is no change in capacitance. This experiment is repeated for different ice thickness until no change in capacitance is observed.
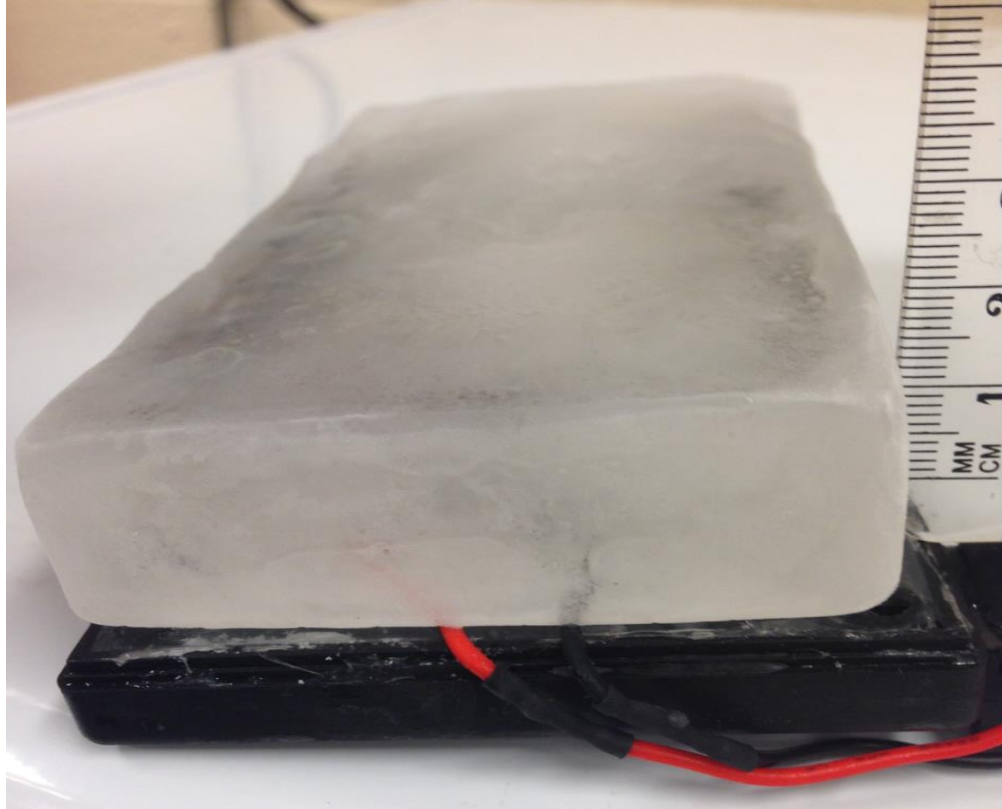
Figure 7.4 Experimental setup using ice slabs (20.5mm)

To calibrate a sensor, a test for repeatability must be performed. For these experiments a new set of runs were performed at the initial stage. Hence the fresh water experiment is repeated three times. Also, new sets of ice slabs were made for each experiment. This is done following the principle of repeatability of experiments as found in Design of Engineering Experiments course EN7516. Also new ice slabs were used so as to get different values of ice thickness and observe the consistency with capacitance obtained for previous experiments.
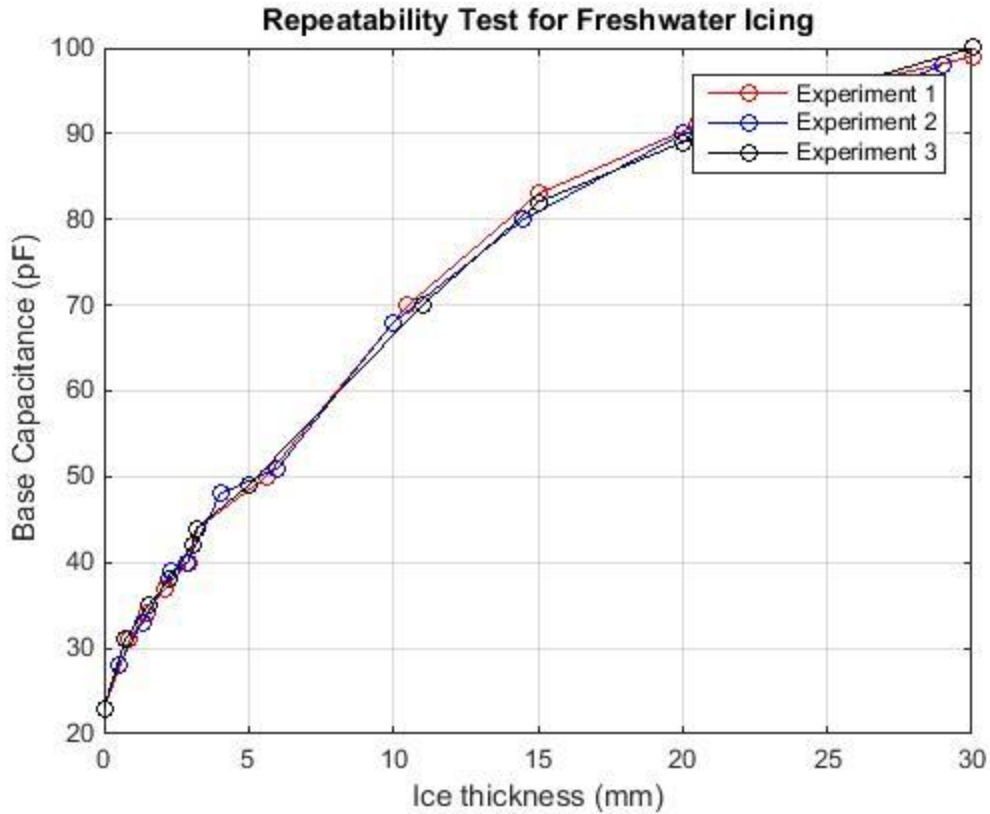
Figure 7.5 Results of 3 Experiments using fresh water

As observed from Figure 7.5 above, the result of the 3 experiments are correlated, the graph shows more consistency at the from 0mm to 5mm where the experiments were performed by spraying water on the surface using a spray bottle. This shows that the ice accretion was more steady and linear than the experiments using the ice slabs from 4mm to 30mm. However, the experimental repeatability results stands true as the 3 experiments shows very similar characterises and can represents a linear point to point mapping between the ice thickens and base capacitance up to 20mm.

Furthermore, the conclusion of the experiments using fresh water led to the validation of the results obtained from the COMSOL simulations. Figure 7.6 compares the simulated data for the second prototype and the experimental 1 data. This plot also shows a high correlation between

the two plots at 0 to 5mm ice thickness. This plot shows a proof that the simulation using COMSOL Multiphysics can be used to design, simulate and build real capacitive based sensor for ice accretion measurement.
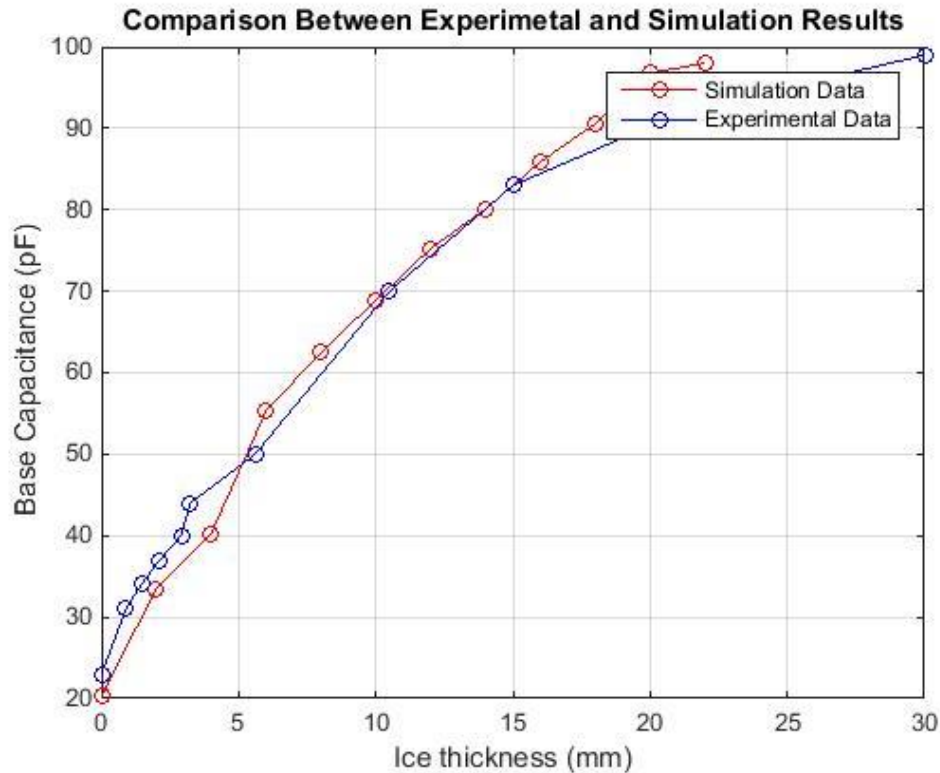
Figure 7.6 Validation Plot for simulation data

7.2.2 Ice accretion results using Sea water

Ocean salinity is important when designing marine icing sensors; hence this creates a need to investigate the change in capacitance using sea water. Sea water is prepared in the laboratory for a salinity of 35 PSU at room temperature as seen in Figure 7.7. The whole solution is brought to about freezing to simulate a typical marine icing environment, and also to gain proper understanding on how temperature would affect freezing in sea water. Similar to the fresh water

experiment, the solution is sprayed evenly on the capacitive sensor plate and left to freeze. More spray is added when there is no change in capacitance and ice thickness is calculated using Equation 7.1.

Figure 7.7 Laboratory preparation of sea water at 20.3^{o}C

Ice layers are added to the surface until complete run off is obtained this is to obtain a consistent ice growth on the surface and also monitor the capacitance for small changes in ice thickness. Figure 7.6 shows the result of the experiments after three spray sessions. Similar to the fresh water experiment for atmospheric icing, the spikes in capacitance as seen on the graph shows the presence of water on the sensing surface, as the relative permittivity of water is much higher than air. Sea water measured up to 100pF initially which is as a result of having more water on the surface forming a small puddle. The setup is placed in a freezer maintained at -18.78∘C, as

freezing occurs, the water change to solid ice and assumes the relative permittivity of ice (~3.2), much higher than air.
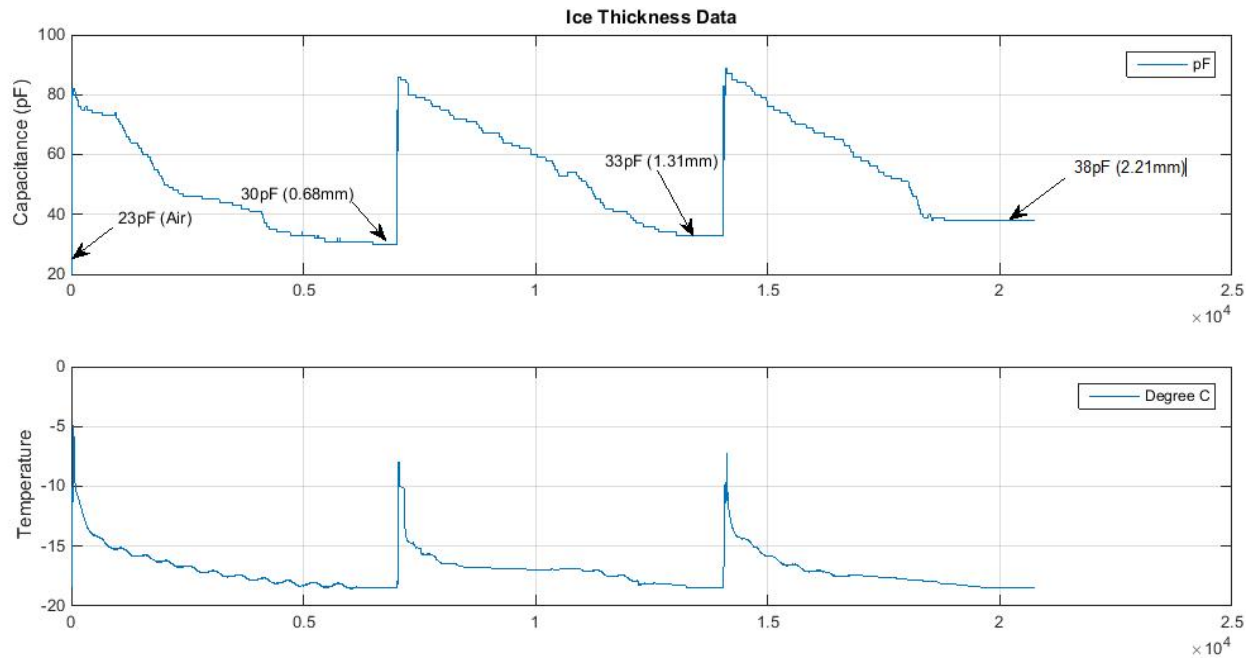
Figure 7.8 Data processing output for ice accretion experiment using Sea water

Further experiments are also performed using ice slabs for larger ice thicknesses that could not produce on the sensor plate by spraying. The ice slab is placed on the sensor plate and the whole setup is placed horizontally into the freezer and monitored until there is no change in capacitance. This experiment is repeated for different ice thickness until no change in capacitance is observed.

The repeatability test is also performed using sea water; hence a fresh experiment is repeated two more times. Figure 7.9 below shows a steady ice increase in capacitance with increase in thickness, for an ideal situation, a linear graph is expected, however due to some experimental and measurement error, some inconsistencies appear in the data. However, the results obtained

are comparable with the fresh water ice accretion graph. A comparison plot between the simulated and experimental data is not documented for saltwater because COMSOL Multiphysics so not have the capability to include salinity in ice models for electrostatic computation.
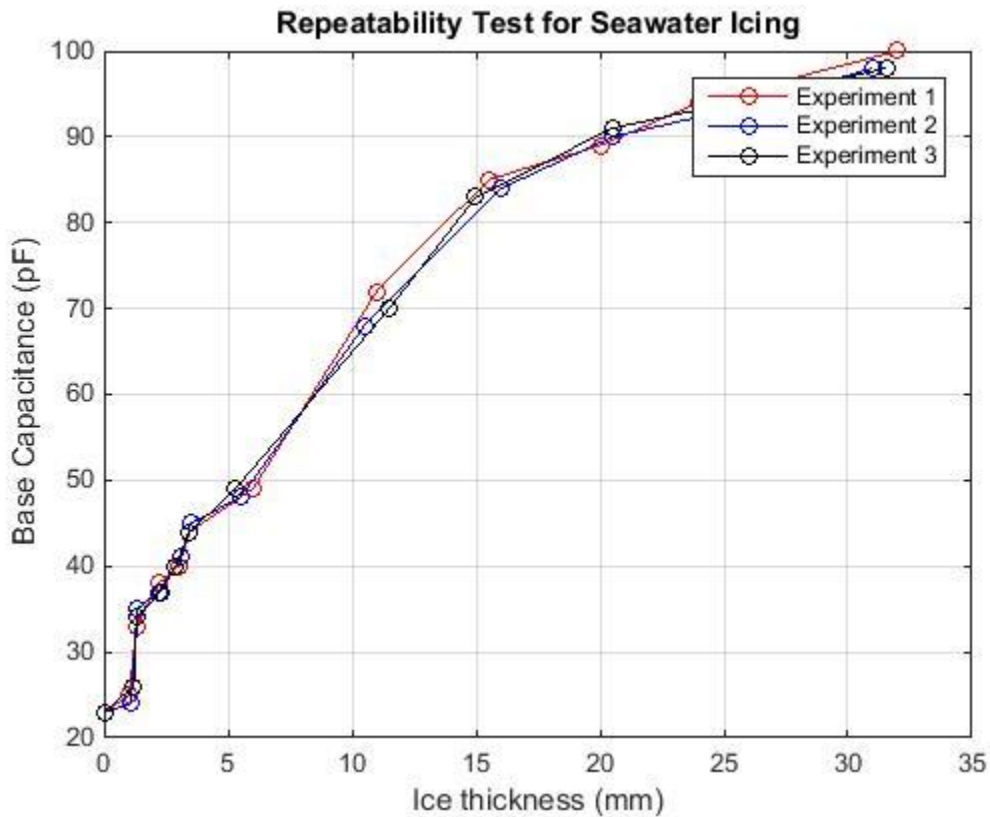
Figure 7.9 Results of 3 Experiments using Seawater (35PSU at Room temperature)

7.3 Experimental Conclusions and Discussions

Controlled experiments were performed using fresh water to obtain atmospheric icing and salt water of 35PSU to simulate sea icing. The experimental measurements are independently collected based on Design of engineering experiments techniques. The ice samples used were made in commercially available deep freezers using tap water with no need further purification

procedure. The change in capacitance shows clear potential due to variation in dielectric property of ice due to increase in thickness. This change in capacitance detected from the ice accretion could be a useful technique in ice accretion detection in harsh marine environments. The freezing of ice shows a physical change from liquid to solid state, and also confirms the difference in dielectric property of ice and water. From the experiments, it is observed that the salt water freezing time is much larger than that of fresh water as expected. The scope of this thesis is not primarily to document the freezing time of either sample; instead, both samples are left to come to the freezer temperature and settled capacitance measurement is recorded. Furthermore, capacitance measurement could not be used to detect salt content in liquid; hence, this sensor could not be used to differentiate between atmospheric icing and sea icing. This experiments shows that both atmospheric and sea icing shows a decrease in the dielectric property as the liquid changes stage. A key conclusion on this experiment shows that the dielectric property of water decreases with an increase in salinity. This is evident in Figure 7.3 and Figure 7.8, initial base capacitance at the beginning of the experimental iterations is much higher in fresh water than in sea water. Gadani *et al* presented a results where salt water between 5000ppt to 35000ppt were measured at a frequency range of 200 MHz to 1.4GHz, results shows that electric property of sea water decrease with an increase in salt concentration. Figure 7.10 shows further analysis from the experiment which shows an increase in dielectric loss with increase in salinity [26].
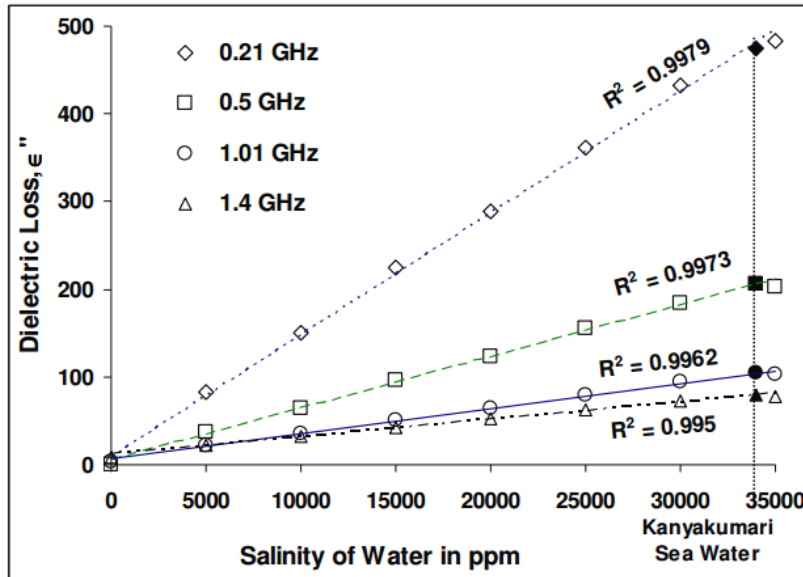
Figure 7.10 Variation of dielectric loss with Salinity

The result of this journal is consistent with the findings in this thesis; the dielectric constant of water is higher in fresh water than in salt water, also the dielectric loss increases as temperature decrease, effectively brining the water to freezing.

7.4 Sensor Calibration

The ice Sensor is calibrated based on point to point linear mapping, for this particular sensor experimented in this thesis, the calibration will be done from 0mm to 15mm. As shown in Figure 7.11 and 8.12 below, the linear range for this calibration is obtained by discarding the last 3 readings where the sensor couldn't show any consistent linear reading, although decent readings could be extended to 20mm, but this might include some erroneous points. For this thesis, the calibration for this sensor will simply be done in the microcontroller C++ attached in APPENDIX B of this report.
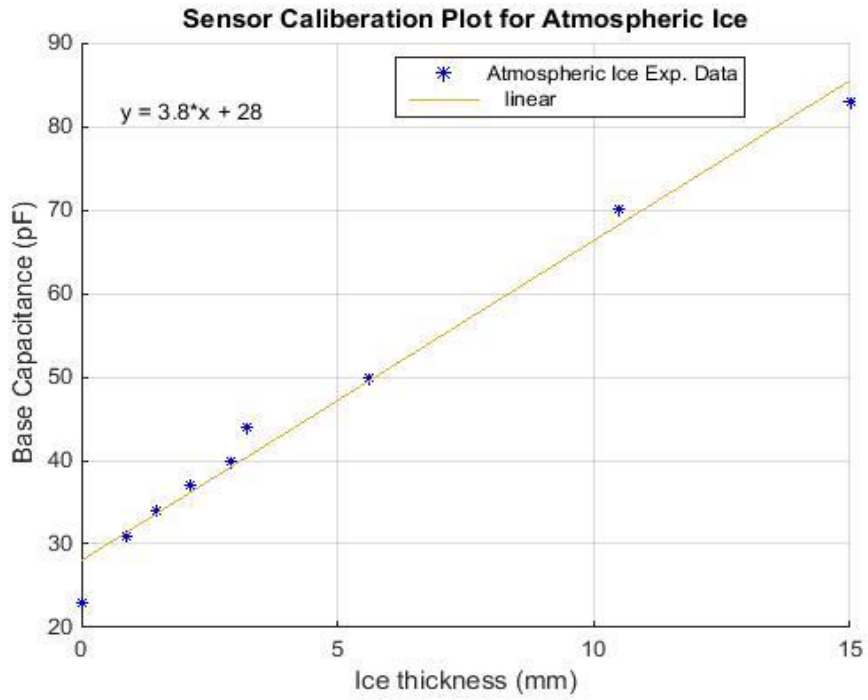
Figure 7.11 Sensor Calibration Plot for freshwater
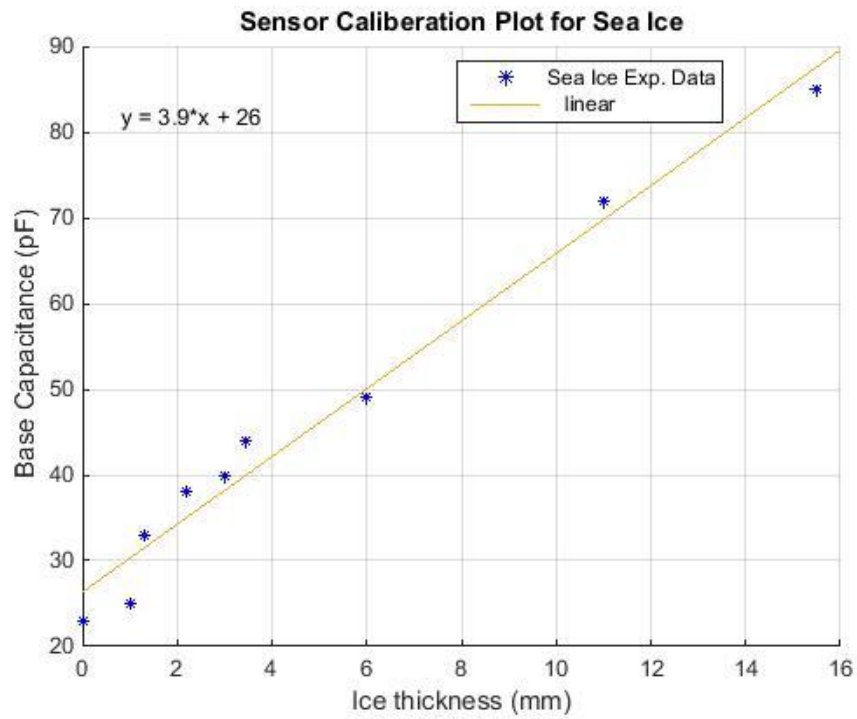
Figure 7.12 Sensor Calibration Plot for seawater

From the above plot the Ice thickness for atmospheric ice can be obtained from the equation

$$Ice\ thickness\ (mm) = \frac{Base\ Capacitance - 28}{3.8} \qquad \text{(7-2)}$$

And the thickness for sea ice can be obtained from the equation

$$Ice\ thickness\ (mm) = \frac{Base\ Capacitance - 26}{3.9} \qquad \text{(7-3)}$$

Again the sensor is calibrated and tested using the equation above; the outcome was very good and contained very little error.

In order to evaluate the correlation between the two equations, the root mean square error of the two equations is computed using:

$$RMSE = \sqrt{\frac{1}{N} \sum_{n=0}^{N-1} (x(n) - y(n))^2} \qquad \text{(7-4)}$$

Where $x(n)$ = Atmospheric Ice data sequence and

$y(n)$ = Sea Ice data sequence.

The RSME of the two sequences is 0.7077 meaning the two data sequences are highly correlated with very little spreads.

Hence, either equation could be used in sensor calibration to obtain a decent result for ice growth.

Some sources of error might include

- Preparing a consistent ice sample could pose some error, during the experiments; ice samples are prepared close or around the dimension of the previous one.

- The pre-made ice thickness is measured using a caliper, and the average measurements from all the four edges were used to determine the thickness of each slab.

Chapter 8

Theoretical Analysis of Multiphase Medium

8.0 Introduction

This Chapter introduces a theoretical analysis of three phase media with a water layer over the ice layer with a layer of spongy ice in-between. This case represents a real scenario of multiple phases being present at the same time. The key objective is to propose a sensing method that can uniquely discriminate predicts the response for each level of ice and water. Our approach is to provide at least two measurements of the same media that are linearly independent from each other. In simple terms, the two characteristics intersect at the solution point, in this case the ice thickness and water film thickness.

8.1 Simulation Methods

The simulation setup is performed in COMSOL Multiphysics for a simple two strip capacitive plates as represented in Figure 8.1. The model setup shows the basic components of the multiphase system with ice layer directly over the electrodes followed by some spongy ice with overlaying water layer. This simulation is to provide a start-up simulation to validate the theoretical conclusion on how changes in air gaps affect the capacitance of the overall setup. Additionally, this analysis also provides a validation for the experimental part of this thesis.
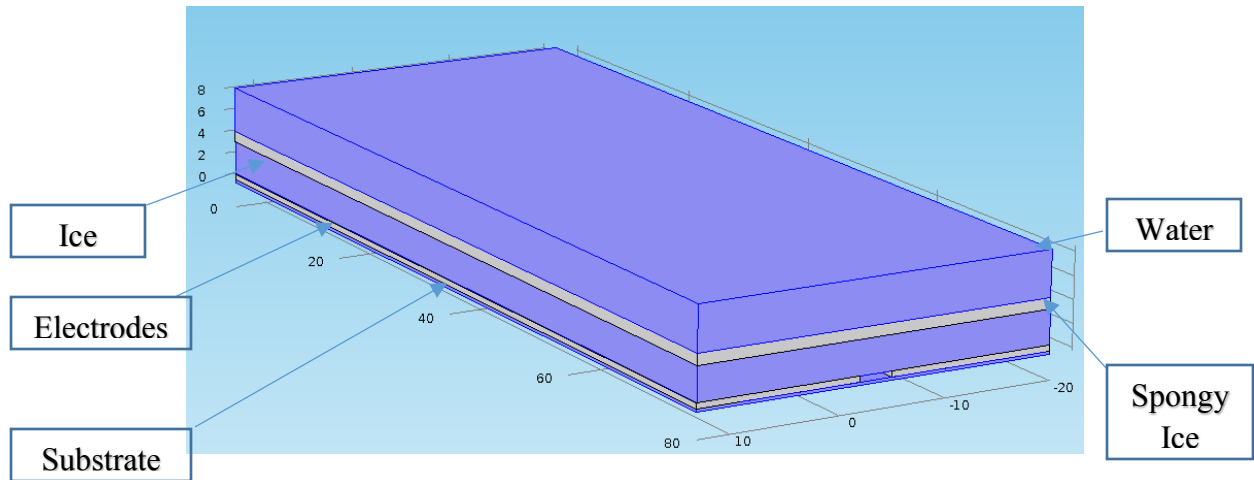
Figure 8.1 Two phase media simulation setup

The system simulation is performed to investigate the capacitance as well as to provide a visual perspective of the basic physics of capacitance sensing as explained in the previous chapter. Figure 8.2 shows the electric filed lines as explained charges moves from less excited medium to a higher one. In other words, the electric filed line originates from the positive plate and terminates in the negative plate. The fringing filed passes through the material places on its path.
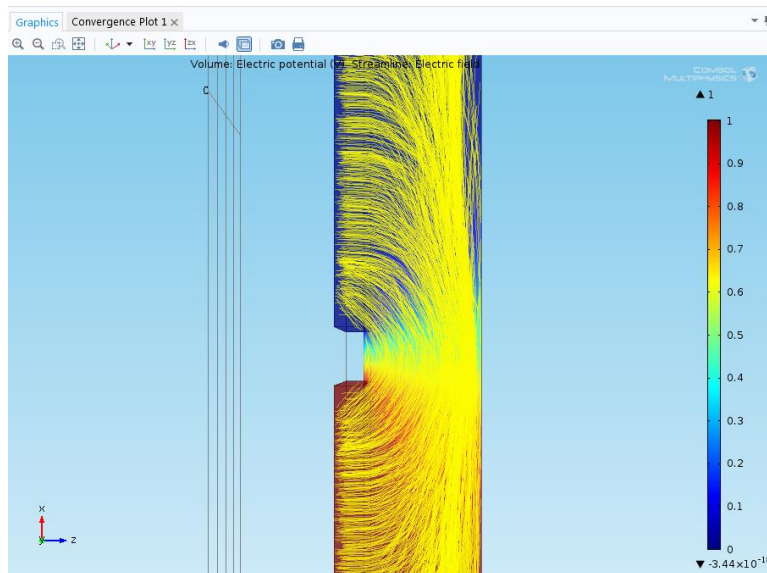
Figure 8.2 Field lines path

In a real marine icing scenario, the ice accretion begins on the super cooled surface, as more sea sprays impinge on the already frozen ice slabs, freezing occurs on the interface, and continues to increase until the whole medium is frozen to solid ice. During this process, some spongy ice is present in-between the solid ice and water interface, which contains a weighted amount of air, water and ice. But for simulation purposes, this thesis will assume a uniform medium of interfacing water and ice with spongy ice sandwiched in-between. The simulation will assume a uniform surface for the whole medium and all other factors in the simulation such as temperature and sensor materials will be constant.

Figure 8.3 below shows the setup for typical 2mm ice, 1mm spongy ice and 2mm water. Closer investigation shows the boundaries between water and ice.
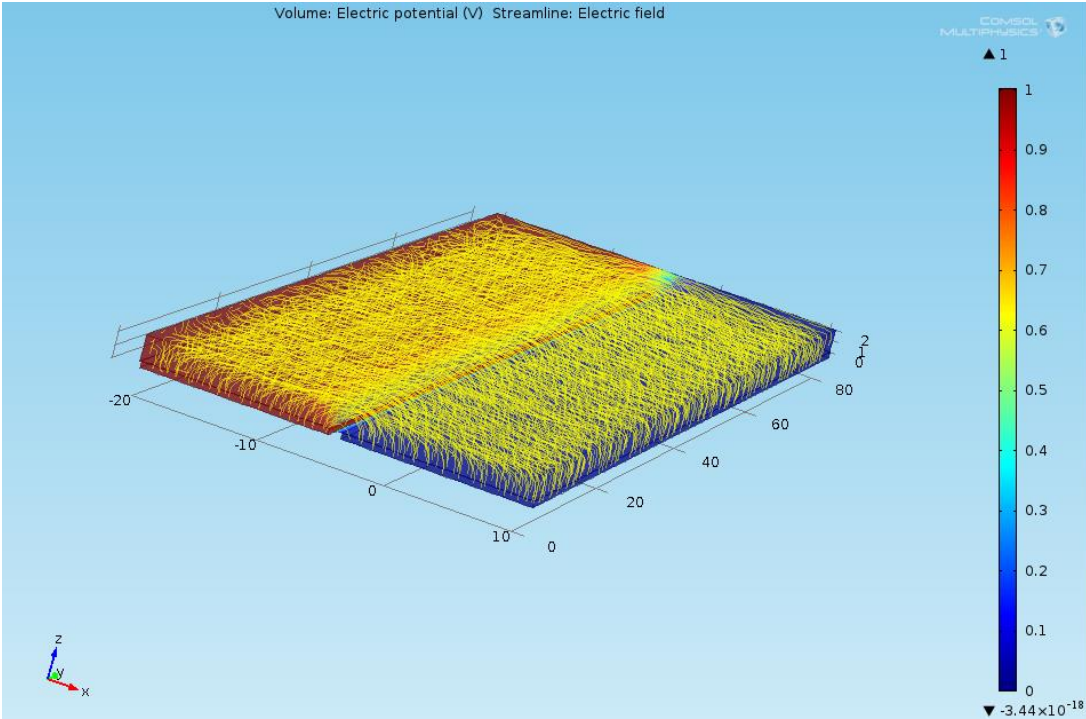
Figure 8.3 Field lines passing through water and ice

8.2 Statistical Design of Experiments

The constituting variables used in most engineering designs are often expressed in terms of various parameters which contribute to the results; these variables are to be investigated to gain knowledge on what parameters are statistically significant. The factors that mainly contribute to the capacitance of this setup are the ice thickness, water thickness, amount of spongy ice and the sensor air gaps. Additionally, the type of material used for the substrate and the electrodes could affect the output capacitance, but for simplicity of this computer experiment, it was assumed that the same copper electrode and silicon substrate is used and kept constant. A computer based experiment is employed to investigate the effect of these factors in the experiment that contribute to the output capacitance; this is because the air gap is hard-to-change as this entire experiment is eventually transitioned into hardware.

The system modelling and finite element analysis is performed in COMSOL Multiphysics, solutions of the PDE solver are observed for each combination of factors. Since there are interactions between factors and changes in one factor affect the output, a more statistical approach is employed. This chapter demonstrates the application of statistical design of experiment (DoE) in the area of capacitance sensing for marine icing; it proofs to be a very important methodology to obtain a model for capacitive sensor in very few experimental runs. The DOE methodology is useful in developing a mathematical model that predicts how input variables interact to generate output variables [19]. Additionally, the model obtained is a representation of the results in terms of the input variables. This report presents a full computer model of the problem and analysis of results and no optimization approach of the system is investigated.

The surface methodology (RSM) is used primarily in this simulation experiment, based on the statistical design of experiments (DoE). This methodology provides more efficient way of studying the main effects of the variables as well as their interactions. An Optimal custom design is chosen because the experiment contains two numeric factors and one categorical hard-to-change factor.

8.2.1 Factors and responsible variables.

The factors chosen in this study are number of critical a resource which determines the output capacitance of a capacitance sensor in a real life scenario. Table 3 shows the variation range or level of factors; as can be seen, each factor has a defined range of study. This study aims at determining capacitances measured for water and ice thicknesses for various airgaps and different quantity of spongy ice in the medium.

Table 3 Factor Levels

Factor Name	Levels				
A=Ice (Numeric)	0	1	2	3	4
A=Ice (Numeric)	0	1	2	3	4
C=Spongy Ice (categorical)	0	0.5	1		
D=air gap (categorical)	1	2	3		

From the previous discussions, the analysis obtained from this study should provide a seamless way of calculating the component factors just buy the knowledge of the output capacitance and the choice of air gap. Additionally, since this is a computer experiment, no replications is required because of the absence of noise; an optimal custom design is used, As seen from Table

4, the full design has 27 runs without replications. The optimal custom design provides a flexible custom model where all possible combination of factors in the experiment is considered.

8.2.2 Statistical analysis of the RSM results

The entire experiment is designed and analysed in Design Experts 9 from Statease. This objective of this analysis is to determine the significance of the input factors as shown in Table 4 The main focus of this part is to determine the significance of the model itself and also to realise a reduced number of factors which will then be used to obtain a response surface design for fitting at least a second order polynomial to result.

Table 4 Data from Simulation experiments

A:Ice	B:Water	C:Spongy Ice	D:Air Gap	Capacitance
3	4	1	1	12.721
3	0	1	3	7.071
0	0	1	3	1.529
4	4	0.5	3	8.899
3	1	1	1	12.15
0	4	0.5	2	8.183
0	4	0	1	28.022
0	1	0	1	18.365
4	0	0	3	6.198
0	4	0	3	25.341
0	1	0.5	3	5.723
1	2	1	2	9.256
2	0	0	1	11.839
0	0	0	2	1.325
0	0	1	1	5.825
4	0	1	2	8.787
0	4	0.5	1	9.502

4	2	0.5	2	9.732
4	4	1	2	10.038
2	2	0.5	1	12.003
0	4	1	3	6.911
3	4	0	2	10.276
0	0	0.5	2	2.537
4	0	0.5	1	11.63
4	3	0	1	12.567
4	2	1	3	8.528
1	3	1	1	12.293

Further analysis of the results is seen in Figure 8.4, the fit summary suggests the best and simplest model for the problem. In this case, design Expert software suggested a quadratic. This shows that the best model to represent the output capacitance in terms of the input will simply be a quadratic. The best model is seen from the highest R^2 value of 0.9919.

Table 5 Statistical analysis results

		Model Summary Statistics				
Source	**Std. Dev.**	**R-Squared**	**Adjusted R-Squared**	**Predicted R-Squared**	**PRESS**	
Linear	4.59	0.5526	0.4184	0.1351	814.94	
2FI	1.50	0.9832	0.9377	0.6421	337.19	
Quadratic	0.54	0.9984	0.9919	0.8924	101.38	Suggested
Cubic					+	Aliased

The ANOVA (Analysis of Variance) test in design Expert 9 is used is for significance analysis, the Figure 8.5 shows individual factors, their interactions and their significance; a significance threshold of 5% is used in this model. In other words, any parameter greater than with "Prob

>F"= 0.05 is insignificant and ignoring it in the equation will have little effect on the response (capacitance). Additionally, since this study conducts an optimal custom design, in which the main effects and interactions are considered, studying the curvature in the RSM is of much importance. The significance of a curvature implies that a second order effect has to be added to the experiment so as to have an adequate regression model. Upon performing ANOVA as shown in Table 5 it reveals that the curvature is insignificant hence no additional point is needed in the experiment.

Table 6 ANOVA Table

Source	Sum of Squares	DF	Mean Square	F Value	p-value Prob > F	
Model	940.73	21	44.80	152.48	< 0.0001	significant
A-Ice	0.11	1	0.11	0.39	0.5603	
B-Water	149.94	1	149.94	510.38	< 0.0001	
C-Spongy Ice	149.11	2	74.55	253.77	< 0.0001	
D-Air Gap	90.26	2	45.13	153.61	< 0.0001	
AB	19.92	1	19.92	67.80	0.0004	
AC	122.02	2	61.01	207.66	< 0.0001	
AD	2.19	2	1.10	3.73	0.1020	
BC	75.61	2	37.80	128.68	< 0.0001	
BD	3.82	2	1.91	6.50	0.0406	
CD	80.45	4	20.11	68.46	0.0001	
A^2	8.60	1	8.60	29.27	0.0029	
B^2	2.43	1	2.43	8.28	0.0347	
Residual	1.47	5	0.29			
Cor Total	942.20	26				

Std. Dev.	0.54	R-Squared	0.9984	
Mean	10.27	Adj R-Squared	0.9919	
C.V. %	5.28	Pred R-Squared	0.8924	
PRESS	101.38	Adeq Precision	54.738	

The ANOVA analysis in Table 6 shows that a quadratic model should be fitted to the data. The Significant factors are B, C, D, AB, AC, BC, BD, and CD. This makes sense as the dielectric property of ice is the lowest out of the other factors; hence it is not very significant in the output capacitance. However, the interaction with water and spongy ice is significant. This provides a useful insight on designing capacitance sensors for marine icing where a significant amount of spongy ice and water is present.

Furthermore, based on the estimated coefficient of the significant factors, the FEM simulated data were fitted to a three dimensional polynomial regression that is listed below:

$$C^i = k_0^i + k_1^i x + k_2^i y + k_3^i xy + k_4^i x^2 + k_5^i y^2 \tag{8-1}$$

Where C: Capacitance (pF)

i: Airgap (mm) and spongy ice combination.

x: ice layer (mm)

y: water layer (mm)

$$0 = -C^i + k_0^i + k_1^i x + k_2^i y + k_3^i xy + k_4^i x^2 + k_5^i y^2$$

$$= F^i(x, y) \tag{8-2}$$

The slope of the constant capacitance characteristics for each air gap is calculated as an implicit function using a F(x,y), using the implicit derivation formula below:

$$\left(\frac{dy}{dx}\right)^i = -\frac{\frac{\partial F}{\partial x}}{\frac{\partial F}{\partial y}} \tag{8-3}$$

The derivative $\left(\dfrac{dy}{dx}\right)^i$ is a function of the solution point (x, y) and five coefficients k_n, n= 1 ~5:

$$\left(\frac{dy}{dx}\right)^i = -\frac{k_1^i + k_3^i y + 2k_4^i x}{k_2^i + k_3^i x + 2k_4^i y} \qquad (8\text{-}4)$$

A close observation of the coefficients reveals that the higher order terms share the same value of

k_3, k_4 and k_5 for all i =1, 2, 3.

This derivative also corresponds to the output of the simulations. Table 8.2 shows the final

quadratic regression coefficients for C obtained from the analysis in coded units.

Table 8.7 Coefficient of the results in terms of the coded values

Coeff.	Airgap=1mm Spongy ice=0mm	Airgap=2mm Spongy ice=0mm	Airgap=3mm Spongy ice=0mm	Airgap=1mm Spongy ice=0.5mm	Airgap=2mm Spongy ice=0.5mm
k_0	+13.84002	+1.58721	+11.67851	+6.15500	+2.46713
k_1	+0.017806	+0.38384	+0.47993	+3.26493	+3.63096
k_2	+4.33958	+4.85508	+4.27396	+1.69440	+2.20990
k_3	-0.38601	-0.38601	-0.38601	-0.38601	-0.38601
k_4	-0.47435	-0.47435	-0.47435	-0.47435	-0.47435
k_5	-0.20274	-0.20274	-0.20274	-0.20274	-0.20274
Coeff.	Airgap=3mm Spongy ice=0.5mm	Airgap=1mm Spongy ice=1mm	Airgap=2mm Spongy ice=1mm	Airgap=3mm Spongy ice=1mm	
k_0	+4.39118	+6.03024	+2.21093	+1.17282	
k_1	+3.72705	+3.10467	+3.47069	+3.56679	
k_2	+1.62879	+2.29596	+2.81146	+2.23034	
k_3	-0.38601	-0.38601	-0.38601	-0.38601	
k_4	-0.47435	-0.47435	-0.47435	-0.47435	
k_5	-0.20274	-0.20274	-0.20274	-0.20274	

The derivatives $\left(\dfrac{dy}{dx}\right)^i$ therefore differ from each other which imply that the characteristics for different air gaps as well as spongy ice thicknesses are linearly independent across the entire domain of ice and water layer thickness under investigation. This confirms the initial hypothesis that an array of two or more sensors of different air gap can be used to uniquely determine the thickness of ice and water. The optimal gap spacing difference will be studied in future. Additionally, the coefficient of the equations shown in Table 8.5 are in terms of the actual factors and can be used to make predictions about the capacitance response for given levels of each factor at some amount of spongy ice.

8.2.2 Validation of RSM Results

The RSM consists of different steps, and the assumption of constant variance need to be validated. Additionally, this is needed to ensure that a useful data is collected from the COMSOL platform. Figure 8.6 shows the plot of standardised residuals, as observed, all the points are aligned on the linear graph line.
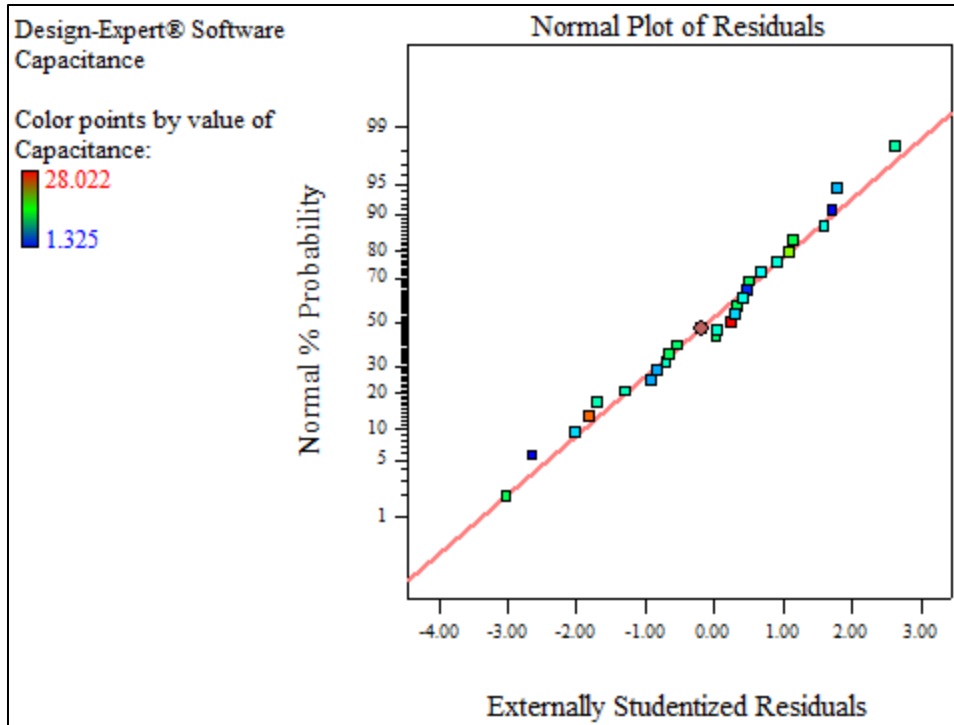
Figure 8.4 Normal probability of residuals

This means the data collected shows no violation to the assumption of constant variance and the errors are normally distributed, also there is no need to apply a transformation to the model. Figure 8.7 is a plot of the residual versus the predicated points collected, for the whole data range, the plot shows that the points are in close correlation and are aligned around the origin; this observation indicates that the model and data collected is adequate.
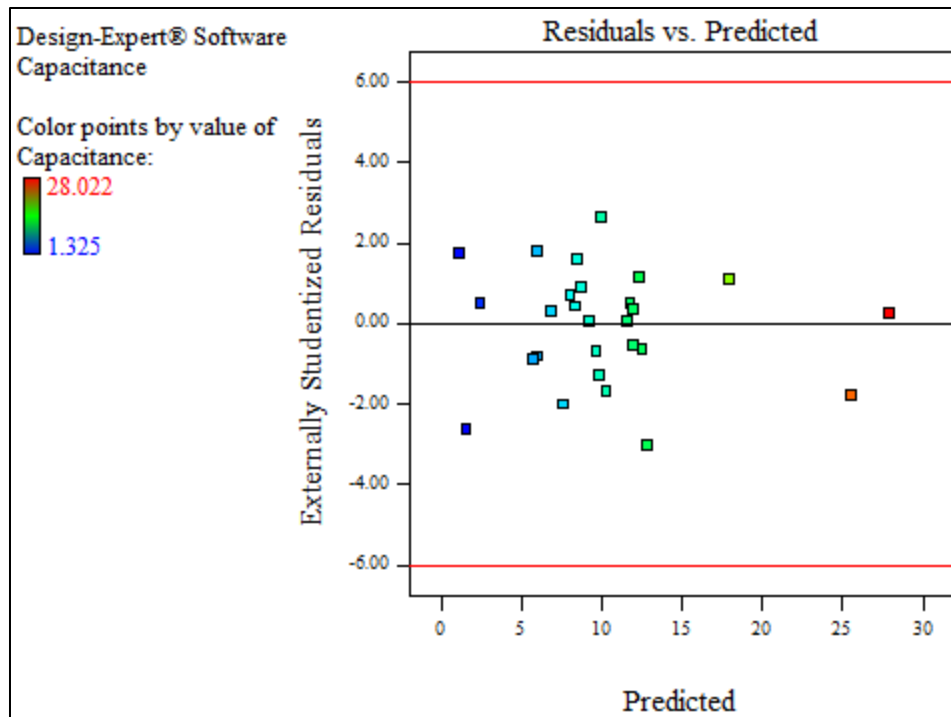
Figure 8.5 Residuals vs. Predicted Plots.

8.3 Response Surface Model.

A second order design is obtained for this analysis. Due to the presence of nonlinearities in the surface of this design, a second order design allows the flexibility to fit a second order regression equation.

There are other second order designs like the central composite design (CCD) and the Box-Behnken design (BBD). For this analysis, a custom RSM is used to accommodate the hard to change factors in the design with the minimal amount of runs. The location of the vertex edge and interior points are already embedded in the design and a Response surface can simply be generated.
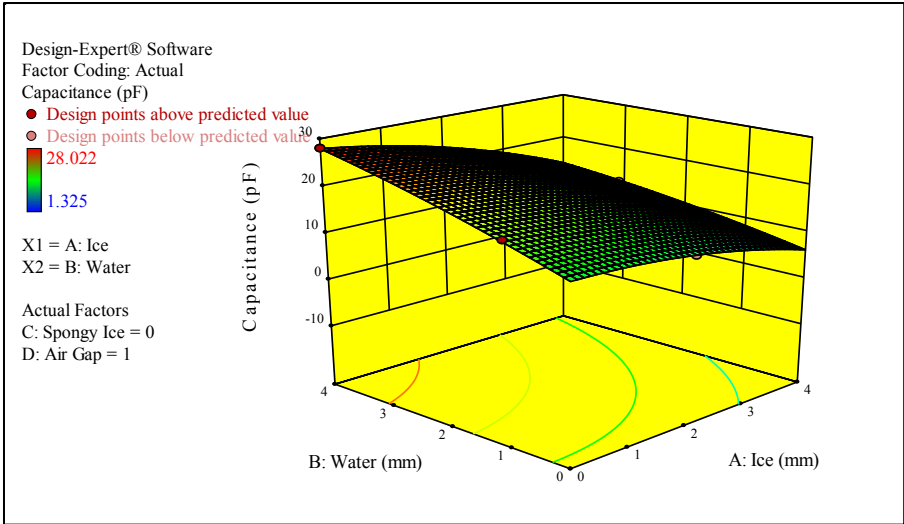
Figure 8.6 3D Capacitance plot for 1mm air gap and 0mm Spongy ice.
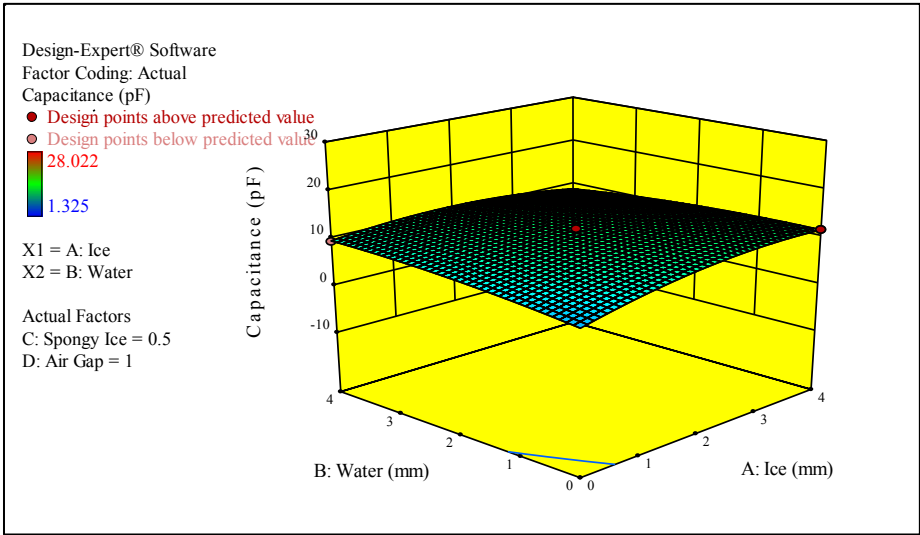
Figure 8.7 3D Capacitance plot for 1 mm air gap 0.5mm spongy ice
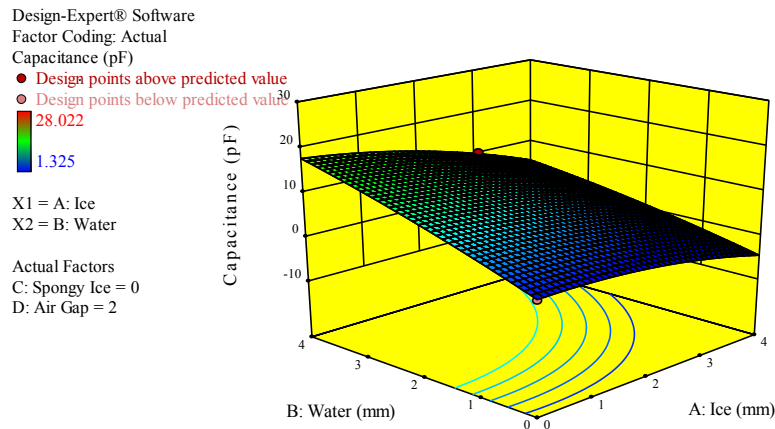
Figure 8.8 3D capacitance plot for 2mm air gap spongy ice 0mm

Figure 8.8 shows that in the absence of spongy ice, an increase in the water layer thickness results in a significant increase in the capacitance, however the capacitance drops off slowly as the ice thickness is increased simultaneously. This effect reduces with an increasing air gap and spongy ice. Also comparing the Figure 8.8 to 8.10 it is evident that the capacitance is highest at an increased water thickens and a reduced ice thickness regardless of the air gap. The capacitance and the length of the field lines got worse with increased air gap. The plots also shows that ice and water layer thickness for different air gaps can determined as the crossing point of two contour plots.

Different combination of spongy ice thickness with air gap shows different capacitance output in the presence of water and ice. To obtain the optimum air gap requirement for a certain sensor, an optimisation analysis should be performed.

8.4 Result Conclusions

This chapter presents a useful application of Statistical using design of Engineering experimental techniques in modelling , validating and analyzing a real life scenario of for a multiphase phase media with ice, water and spongy ice interaction. This research strives to conduct design of experiment for determining a suitable air gap for a particular marine icing application for ice, water and spongy ice measurement to produce the best results in a real world marine icing phenomena.

The applied method proofs that the applied model is statistically significant and an increase in the water layer will increase the capacitance significantly regardless of the air gap used. Furthermore, the results also shows that the air gaps for such an application should be around 2mm or less since is it measures more capacitance, hence longer and more direct electric field lines.

The method also proves that different sensors of different air gap can be used to uniquely determine the thickness of ice and water using the proposed model and a uniquely independent fitted curve on a Response surface model. Conclusions and observations deduced from this chapter are applied in the marine icing sensor design elaborated in the subsequent chapters.

Chapter 9

Conclusion

9.0 Research Conclusion

A capacitive based Marine icing sensor developed in Memorial University of Newfoundland Electrical and Electronics Laboratory and tested in the Hydro fluids laboratory. This system was developed in collaboration with Statoil Canada Limited, RDC and MITACS. This system is capable detecting ice thickness on a surface within acceptable accuracy.

In this thesis, three different geometry of capacitive sensor plate is simulated, fabricated and, tested; the basic characteristics of the sensor plates were analyzed by studying the electrical properties of the sensor tracings. Electric field lines behaviour, sensor geometry and materials were also investigated to produce the best possible sensor for marine icing. FEM software is also used in simulating two phase and multi-phase icing phenomena, experimentally validated in this thesis.

Charged copper tracings on silicon substrate can be used in material detection by electrically exciting one end of the copper tracing and the other end grounded, this produces an electric field lines which is broken by the material in the vicinity. In this thesis, a low cost, low power consumption capacitance to digital converter circuitry is proposed and built. The capacitance to digital converter excites the capacitive plates and digitized. The resulting digital vales of the capacitance are read using a low cost microcontroller available on board. Experiments shows that

the proposed system can measure ice thicken in real time. The proposed system can be modified for installation for ice detection and can be easily integrated to trigger heat tracing to melt ice.

9.1 Research Contribution

The overall research is an industrial collaboration for a system deployable to monitor marine icing on deck of offshore vessels and rigs. This thesis is also a contribution to sensor technology as a means to explore more on capacitive sensing in the area of marine technology. The contributions of this research are as follows:

- The research laid a foundation for effective marine icing sensing using capacitive technique. Marine icing sensing for a single phase steady state condition was experientially verified.

- Design of Engineering Experiments (DoE) based method of analyzing and modeling multiphase medium of water and ice, with spongy ice embedded in-between. The FEM data proof linear independence of three different air gap sensors and the solution of a given ice and water thickness are determined as the crossing point of contour plots.

- This thesis presents a prototype of a standalone, fully operational, RMI resistant marine icing sensor, capable of detecting ice thickness has been designed in this thesis.

- Three different copper tracing sensor geometries is designed and simulated in COMSOL Multiphysics; two comb type and one circular hatched type sensor. The comb type has the electric field line parallel to the comb fingers and the last prototype has the electric field distributed in a circular pattern and centered in the middle of the Sensor plate.

- Simple, low cost and low power micro controller based circuitry for capacitance to digital conversion is developed and tested in the Electronics lab at Memorial University of Newfoundland.

- Experimental proof of dielectric loss with increase in salinity.

- Valuable ice thickness data for both fresh and salt water are obtained using the proposed ice sensor. Necessary documentation of all engineering procedures including results is contained in this thesis.

9.2 Future Work

The work presented in this thesis is part of a large research area in marine sensing in general. The result and conclusion resented in this thesis is to provide a starting point on the application of capacitive sensing in marine icing detection, quantifying and removal of ice loads in offshore vessels and rigs. This thesis also draws more attention on capacitive sensing as a replacement for more expensive direct or indirect ice sensing techniques like ultrasonic, inductive and image processing. Some of the future work could be developed and documented as follows.

- The optimal air gap could be investigated in the future using the RSM optimization tool available in design expert 9 software, this will provide a more refined method which provides the best air gap for measuring a given ice thickness.

- Testing different sensor arrangement for improved sensitivity.

- This thesis contains full detail of the electronics schematics ready for PCB design. It is possible to use this documentation in producing a PCB of this sensor, end product will be rugged and ready to use for offshore vessels and rigs.

- The Sensor plate presented in this thesis provides a starting point to assist in further exploration of highly sensitive sensor geometry that could produce electric field lines long enough to detect ice thickness more than 30mm. This will be very useful in offshore Marine icing detection where ice loads range from 20mm to 300mm.

- Methods to integrate the sensor with defrost system should also be investigated.

- Both the sensing plate and the sensor electronics can be enhanced using Micro-Electro-Mechanical Systems Technology (MEMS) this will produce a miniaturized version of the whole system that is even more easily deployable and easy to modify.

Bibliography

[1] D. o. N. Resources, "Government of Newfoundland and Labrador," 29 July 2015. [Online]. Available: http://www.nr.gov.nl.ca/nr/energy/statistics/peschart.html. [Accessed 8 March 2016].

[2] C. C. guard, "Government of Canada," 24 June 2013. [Online]. Available: http://www.ccg-gcc.gc.ca/e0010733. [Accessed 8 March 2016].

[3] A. Dehghani-sanij , "Analysis of ice accretion on vertical surfaces of marine vessels and structures in arctic conditions," in *OMAE2015*, St. John's, 2015.

[4] F. S., "Atmospheric Icing on Structures measurement and data collection on icing state of the art," MetroSwiss, Oslo, 2006.

[5] W. Li, H. Zhang, L. Ye and Y. Zheng , "Fiber-Optic Ice Detection System for Aeroplane application," Department of Control Science & Engineering , Wuhan, China, 2004.

[6] R. A. Inc., "Goodrich Ice Detector Models 0871LH1," UTC Aerospace Systems , Burnsville, 2013.

[7] C. AB, "Ice monitor," SAAB Technologies , Östersund , 2003.

[8] S. Inkpen, C. Nolan and M. M. Oleskiw, "Development of a sensor for the detection of atmoshpheric ice," in *5th IWAIS*, Tokyo, 2005.

[9] *Instrumar,* St John's: Instrumar, 2014.

[10] *Notes from HoloOptics,* Narvik: HoloOptics, 2001.

[11] M. Tiuri, S. A, N. F and . H. M, "The Complex Dielectric Constant of Snow at Microwave," *IEEE JOURNAL OF OCEANIC ENGINEERING,* vol. 9, no. 5, pp. 377-382, 1984.

[12] E. S, "“Dielectric properties of ice and snow - a Review," *Journal of Glaciology,* vol. 5, no. 42, pp. 779-779, 1965.

[13] W. M. L, "Ice sensor". United states Patent US Patent 4766369, 1988.

[14] O. K.P, "Capacitive probe for ice detection and accretion rate measurement: Proof of concept," in *Masters thesis report submitted at University of Mannitoba* , Mannitoba , 2010.

[15] J. P.O, "“Total impedience and complex dielectric property ice detection System". Unites States Patent US Patent 7439877, 2008.

[16] B. Wichura, "A Survey of Icing Measurements in Germany," in *IWAIS XII,* , Potsdam, 2007.

[17] H. Semat and R. Katz, "Research Papers in Physics and Astronomy," in *Capacitance and Dielectrics*, Nebraska, Robert Katz, 1998, pp. 461-487.

[18] L. K. Baxter, "Capacitive sensors, design and applications," in *IEEE Press*, New York, 1997.

[19] e. a. R.D. Watkins, *Ice Detector,* 1986.

[20] T. Instrument, "Basics of Capacitive Sensing and Applications," Texas Instrument Incorporated, 2014.

[21] D. Wang, "FDC1004: Basucs of Capacitive Sensing and Applications," Texas Instrument ,

2014.

[22] C. Multiphysics, *Version 4.2. COMSOL, Inc.,* Burlington, MA, USA. , 2011.

[23] F. N. Toth, A. M. Bertels and G. Meijer, "A low-cost, stable reference capacitor for capacitive sensor systems," *IEEE Trans. Instrum. Meas.,* vol. 45, no. 2, pp. 526-530, April 1996.

[24] A. HEIDARY, "A Low-Cost Universal Integrated Interface for capacitive Sensors," Iran , 2010.

[25] D. Gadani, V. A. Rana, S. P. Bhatnagar, A. N. Prajapati and A. D. Vyas, "Effect of Salinity on dielectic property of water," *Indian Journal of Pure and Applied physics,* vol. 50, no. 1, pp. 405-410, 2012.

[26] M. D.C, Design and Analysis of Experiments, fifth ed, New York: Wiley, 2005.

[27] *MATLAB documentation,* 2013.

[28] F. Reverter, X. LI and G. Meijer, "Stability and accuracy of active shielding for grounded capacitive," *Meassurement Science and Technology,* vol. 17, pp. 2884-2890, 2006.

[29] F. Reverter, X. LI and G. Meijer, "A novel interface circuit for grounded capacitive sensors with feedforward-based active shielding," in *Measurement Science and technology*, Feb 2008.

Appendix A

A.1 Capacitance to Digital Conversion and Temperature Sensing

```
#include <OneWire.h>
#include <Wire.h>
#include <FDC1004.h>
OneWire ds(4);  // DS18S20 Temperature chip

FDC1004 fdc; //Or, specify a rate: 100HZ, 200HZ, and 400HZ
FDC1004 fdc(FDC1004_400HZ)

void setup(void) {  //initialize inputs/outputs
Wire.begin();  // start serial port
  Serial.begin(115200);
}

void loop(void) {

  //For conversion of raw data to C
  int HighByte, LowByte, TReading, SignBit, Tc_100, Whole, Fract;
  int32_t capacitance = fdc.getCapacitance(0)/1000;

  byte i;
  byte present = 0;
  byte data[12];
  byte addr[8];

  if ( !ds.search(addr)) {
     //Serial.print("**Sensor Detected**");
     ds.reset_search();
     return;
  }

  if ( OneWire::crc8( addr, 7) != addr[7]) {
     Serial.print("CRC is not valid!\n");
     return;
  }

  ds.reset();
  ds.select(addr);
  ds.write(0x44,1);         // start conversion, with parasite power on at the end
```

```
  delay(1000);           // Initiate some delay

  present = ds.reset();
  ds.select(addr);
  ds.write(0xBE);        // Read Scratchpad


  Serial.print(" ");
  for ( i = 0; i < 9; i++) {        //  9 bytes
    data[i] = ds.read();
  }
  LowByte = data[0];   //Conversion of raw data to C
  HighByte = data[1];
  TReading = (HighByte << 8) + LowByte;
  SignBit = TReading & 0x8000;  // test most sig bit
  if (SignBit) // negative
  {
    TReading = (TReading ^ 0xffff) + 1; // 2's comp
  }
  Tc_100 = (6 * TReading) + TReading / 4;    // multiply by (100 * 0.0625) or 6.25

  Whole = Tc_100 / 100;  // separate off the whole and fractional portions
  Fract = Tc_100 % 100;


  if (SignBit) // If its negative
  {
    Serial.print("-");
  }
  Serial.print(Whole);
  Serial.print(".");
  if (Fract < 10)
  {
    Serial.print("0");
  }
  Serial.print(Fract);   //End conversion to C
  Serial.print(" , ");
  Serial.println(capacitance);
  delay(250);
  //Serial.print(" pF\n");

}
```

A.2 FDC1004 Library

```
#include <FDC1004.h>

#define FDC1004_UPPER_BOUND ((int16_t) 0x4000)
#define FDC1004_LOWER_BOUND (-1 * FDC1004_UPPER_BOUND)

uint8_t MEAS_CONFIG[] = {0x08, 0x09, 0x0A, 0x0B};
uint8_t MEAS_MSB[] = {0x00, 0x02, 0x04, 0x06};
uint8_t MEAS_LSB[] = {0x01, 0x03, 0x05, 0x07};
uint8_t SAMPLE_DELAY[] = {11,11,6,3};

FDC1004::FDC1004(uint16_t rate){
  this->_addr = 0b1010000; // Configuring FDC1004 address
  this->_rate = rate;
}

void FDC1004::write16(uint8_t reg, uint16_t data) {
  Wire.beginTransmission(_addr);
  Wire.write(reg); //send address
  Wire.write( (uint8_t) (data >> 8));
  Wire.write( (uint8_t) data);
  Wire.endTransmission();
}

uint16_t FDC1004::read16(uint8_t reg) {
  Wire.beginTransmission(_addr);
  Wire.write(reg);
  Wire.endTransmission();
  uint16_t value;
  Wire.beginTransmission(_addr);
  Wire.requestFrom(_addr, (uint8_t)2);
  value = Wire.read();
  value <<= 8;
  value |= Wire.read();
  Wire.endTransmission();
  return value;
}

uint8_t FDC1004::configureMeasurementSingle(uint8_t measurement, uint8_t channel, uint8_t
capdac) {
    //Verify data
```

```cpp
    if (!FDC1004_IS_MEAS(measurement) || !FDC1004_IS_CHANNEL(channel) || capdac >
FDC1004_CAPDAC_MAX) {
        Serial.println("bad configuration");
        return 1;
    }

    //build 16 bit configuration
    uint16_t configuration_data;
    configuration_data = ((uint16_t)channel) << 13; //CHA
    configuration_data |=  ((uint16_t)0x04) << 10; //CHB disable / CAPDAC enable
    configuration_data |= ((uint16_t)capdac) << 5; //CAPDAC value
    write16(MEAS_CONFIG[measurement], configuration_data);
    return 0;
}

uint8_t FDC1004::triggerSingleMeasurement(uint8_t measurement, uint8_t rate) {
  //verify data
    if (!FDC1004_IS_MEAS(measurement) || !FDC1004_IS_RATE(rate)) {
        Serial.println("bad trigger request");
        return 1;
    }
    uint16_t trigger_data;
    trigger_data = ((uint16_t)rate) << 10; // sample rate
    trigger_data |= 0 << 8; //repeat disabled
    trigger_data |= (1 << (7-measurement)); // 0 > bit 7, 1 > bit 6, etc
    write16(FDC_REGISTER, trigger_data);
}

/**
 * Check if measurement is done, and read the measurement in value
 * Return 0 if successful, 1 if bad request, 2 if measurement did not complete.
 * Value should be at least 4 bytes long (24 bit measurement)
 */
uint8_t FDC1004::readMeasurement(uint8_t measurement, uint16_t * value) {
    if (!FDC1004_IS_MEAS(measurement)) {
        Serial.println("bad read request");
        return 1;
    }
    //check if measurement is complete
    uint16_t fdc_register = read16(FDC_REGISTER);
    if (! (fdc_register & ( 1 << (3-measurement)))) {
        Serial.println("measurement not completed");
        return 2;
    }
  //read the value
  uint16_t msb = read16(MEAS_MSB[measurement]);
```

```
  uint16_t lsb = read16(MEAS_LSB[measurement]);
  value[0] = msb;
  value[1] = lsb;
  return 0;
}

/**
 * Convenience method to take a measurement, uses the measurement register equal to the
channel number
*/
uint8_t FDC1004::measureChannel(uint8_t channel, uint8_t capdac, uint16_t * value) {
  uint8_t measurement = channel; //4 measurement configs, 4 channels, seems fair
  if (configureMeasurementSingle(measurement, channel, capdac)) return 1;
  if (triggerSingleMeasurement(measurement, this->_rate)) return 1;
  delay(SAMPLE_DELAY[this->_rate]);
  return readMeasurement(measurement, value);
}

/**
 * High level function to get the capacitance from a channel.
 * Attempts to manage capdac automagically
*/
int32_t FDC1004::getCapacitance(uint8_t channel) {
  fdc1004_measurement_t value;
  uint8_t result = getRawCapacitance(channel, &value);
  if (result) return 0x80000000;

  int32_t capacitance = ((int32_t)ATTOFARADS_UPPER_WORD) * ((int32_t)value.value);
  capacitance /= 1000; //femtofarads
  capacitance += ((int32_t)FEMTOFARADS_CAPDAC) * ((int32_t)value.capdac);
  return capacitance;
}

/**
 * High level function to get the raw capacitance from a channel
 * Managing CAPDAC
*/
uint8_t FDC1004::getRawCapacitance(uint8_t channel, fdc1004_measurement_t * value) {
  if (!FDC1004_IS_CHANNEL(channel)) return 1;
  value->value = 0x7FFF;
  uint16_t raw_value[2];
  value->capdac = this->_last_capdac[channel]; //load last capdac as starting point

  //sample until we get a good result
  while(value->value > 0x7E00 || value->value < 0x8100) {
    if (measureChannel(channel, value->capdac, raw_value)) {
```

```cpp
            Serial.println("error");
            return 1;
        }
        value->value = (int16_t)raw_value[0];

        //adjust capdac if necessary
        if (value->value > FDC1004_UPPER_BOUND && value->capdac <
FDC1004_CAPDAC_MAX) {
            value->capdac++;
        } else if (value->value < FDC1004_LOWER_BOUND && value->capdac > 0) {
            value->capdac--;
        } else {
            //out of range, but capdac is already maxed (or minned). Return.
            this->_last_capdac[channel] = value->capdac;
            return 0;
        }
    }
    this->_last_capdac[channel] = value->capdac;
    return 0;

}
```

A.3 FDC1004 Header File

```
#ifndef _FDC1004
#define _FDC1004

#include "Arduino.h"
#include "Wire.h"

//Constants and limits for FDC1004
#define FDC1004_100HZ (0x01)
#define FDC1004_200HZ (0x02)
#define FDC1004_400HZ (0x03)
#define FDC1004_IS_RATE(x) (x == FDC1004_100HZ || \
                x == FDC1004_200HZ || \
                x == FDC1004_400HZ)

#define FDC1004_CAPDAC_MAX (0x1F)

#define FDC1004_CHANNEL_MAX (0x03)
#define FDC1004_IS_CHANNEL(x) (x >= 0 && x <= FDC1004_CHANNEL_MAX)

#define FDC1004_MEAS_MAX (0x03)
#define FDC1004_IS_MEAS(x) (x >= 0 && x <= FDC1004_MEAS_MAX)

#define FDC_REGISTER (0x0C)

#define ATTOFARADS_UPPER_WORD (457) //number of attofarads for each 8th most LSB
(lsb of the upper 16 bit half-word)
#define FEMTOFARADS_CAPDAC (3028) //number of femtofarads for each LSB of the
capdac

typedef struct fdc1004_measurement_t{
    int16_t value;
    uint8_t capdac;
}fdc1004_measurement_t;

class FDC1004 {
 public:
    FDC1004(uint16_t rate = FDC1004_100HZ);
    int32_t getCapacitance(uint8_t channel = 1);
    uint8_t getRawCapacitance(uint8_t channel, fdc1004_measurement_t * value);
    uint8_t configureMeasurementSingle(uint8_t measurement, uint8_t channel, uint8_t capdac);
    uint8_t triggerSingleMeasurement(uint8_t measurement, uint8_t rate);
    uint8_t readMeasurement(uint8_t measurement, uint16_t * value);
    uint8_t measureChannel(uint8_t channel, uint8_t capdac, uint16_t * value);
```

```cpp
 private:
   uint8_t _addr;
   uint8_t _rate;
   uint8_t _last_capdac[4];
   void write16(uint8_t reg, uint16_t data);
   uint16_t read16(uint8_t reg);
};

#endif
```

B.2 Data Acquisition Python Codes

```python
# Marine Ice Sensor Data Acquisition code for capacitance and temperature
# Written by Charles Ezeoru

import serial # import Serial Library
import numpy  # Import numpy
import matplotlib.pyplot as plt #import matplotlib library
from drawnow import *

Fract= []
capacitance=[]
arduinoData = serial.Serial('com16', 115200) #Creating our serial object named arduinoData
plt.ion() #Tell matplotlib you want interactive mode to plot live data
cnt=0

def makeFig(): #Create a function that makes our desired plot
    plt.ylim(20,30)                                     #Set y min and max values
    plt.title('My Live Streaming Sensor Data')          #Plot the title
    plt.grid(True)                                       #Turn the grid on
    plt.ylabel('Temperature')                            #Set ylabels
    plt.plot(Fract, 'ro-', label='Degrees C')            #plot the temperature
    plt.legend(loc='upper left')                         #plot the legend
    plt2=plt.twinx()                                     #Create a second y axis
    plt.ylim(0,100)                                      #Set limits of second y axis- adjust to
                                                          readings you are getting
    plt2.plot(capacitance, 'b^-', label='capacitance (pF)') #plot capacitance data
    plt2.set_ylabel('Capacitance (pF)')                  #label second y axis
    plt2.ticklabel_format(useOffset=False)               #Force matplotlib to NOT autoscale y axis
    plt2.legend(loc='upper right')                       #plot the legend


while True: # While loop that loops forever
    while (arduinoData.inWaiting()==0): #Wait here until there is data
        pass #do nothing
    arduinoString = arduinoData.readline()          #read the line of text from the serial port
    dataArray = arduinoString.split(',')            #Split it into an array called dataArray
    temp = float( dataArray[0])        #Convert first element to floating number and put in temp
    P =   float( dataArray[1])          #Convert second element to floating number
    Fract.append(temp)                 #Build our temp array by appending temp readings
    capacitance.append(P)               #Building our capacitance array by appending T readings
    drawnow(makeFig)                    #Call drawnow to update our live graph
    plt.pause(.000001)                  #Pause Briefly. Important to keep drawnow from crashing
    cnt=cnt+1
```

```
if(cnt>50):                    #If you have 50 or more points, delete the first one from the array
    Fract.pop(0)               #This allows us to just see the last 50 data points
    capacitance.pop(0)
```